J. Math. Anal. Appl. 383 (2011) 522–540

Contents lists available at ScienceDirect

Journal of Mathematical Analysis and Applications

www.elsevier.com/locate/jmaa

A multigrid-based preconditioned Krylov subspace method for the Helmholtz equation with PML ☆

Zhongying Chen [1], Dongsheng Cheng *, Wei Feng, Tingting Wu, Hongqi Yang [1]

Department of Scientific Computing and Computer Applications, Sun Yat-Sen University, Guangzhou 510275, PR China

ARTICLE INFO

Article history:
Received 29 November 2010
Available online 31 May 2011
Submitted by P. Broadbridge

Keywords:
Helmholtz equation
PML
Krylov subspace method
Preconditioner
Multigird
Interpolation operator

ABSTRACT

In this paper, we generalize the complex shifted Laplacian preconditioner to the complex shifted Laplacian-PML preconditioner for the Helmholtz equation with perfectly matched layer (Helmholtz-PML equation). The Helmholtz-PML equation is discretized by an optimal 9-point difference scheme, and the preconditioned linear system is solved by the Krylov subspace method, especially by the biconjugate gradient stabilized method (Bi-CGSTAB). The spectral analysis of the linear system is given, and a new matrix-based interpolation operator is proposed for the multigrid method, which is used to approximately invert the preconditioner. The numerical experiments are presented to illustrate the efficiency of the preconditioned Bi-CGSTAB method with the multigrid based on the new interpolation operator, also, numerical results are given for comparing the performance of the new interpolation operator with that of classic bilinear interpolation operator and the one suggested in Erlangga et al. (2006) [10].

1. Introduction

The Helmholtz equation governs wave propagations and scattering phenomena arising in many areas, for example, in aeronautics, marine technology, geophysics and optical problems.

To solve the Helmholtz equation, absorbing boundary conditions are often used to truncate the infinite domain into a finite domain. In this paper, the perfectly matched layer (PML, cf. [3,7,14]) is used to truncate the domain. The technique of PML was proposed by Bérenger in 1994 [3]. It is an artificial absorbing boundary condition, which has the astonishing property of generating almost no reflection at the interface between the interior medium and the artificial absorbing medium. We call the Helmholtz equation with perfectly matched layer the Helmholtz-PML equation. To discretize the Helmholtz-PML equation, difference methods are usually preferred because of their easy implementation and less computational complexity. The rotated 9-point scheme is a popular method, which needs less grids per wavelength than the conventional 5-point difference scheme while maintaining the comparable accuracy [17,25]. In [6] we analyze the defect of the rotated 9-point finite difference scheme, and present an optimal 9-point finite difference scheme for the Helmholtz-PML equation. Based on minimizing the numerical dispersion, we propose global and refined choice strategies for choosing optimal parameters of the difference scheme.

☆ This research is partially supported by the Science and Technology Section of SINOPEC and Guangdong Provincial Government of China through the "Computational Science Innovative Research Team" program.

* Corresponding author.
E-mail addresses: lnsczy@mail.sysu.edu.cn (Z. Chen), dongsheng2001@sohu.com (D. Cheng), fengw@mail.sysu.edu.cn (W. Feng), wttxrm@126.com (T. Wu), mcsyhq@mail.sysu.edu.cn (H. Yang).

[1] Supported in part by the Natural Science Foundation of China under grants 10771224 and 11071264.

0022-247X/$ – see front matter
doi:10.1016/j.jmaa.2011.05.054

After discretization, when the resulting linear system is extremely large, direct methods cannot serve well, and the Krylov subspace iterative methods, such as Bi-CGSTAB [13,29] and GMRES (the generalized minimal residual method) [21], become good choices. However, these methods are not competitive without precondition, a good preconditioner should be incorporated. This leads to the preconditioned Krylov subspace methods. It has been proved that Krylov subspace methods such as Bi-CGSTAB and GMRES are particularly efficient for systems with a Hermitian positive definite matrix, or more generally, for systems with a coefficient matrix which has a clustered spectrum away from the origin in the right half of the complex plane. As we know, the matrix obtained from discretization of the Helmholtz operator is indefinite, it has a poor spectral distribution which is not beneficial for the convergence of Krylov subspace method. Thus, it has to be preconditioned appropriately.

Many authors contributed to the development of preconditioner for the Helmholtz equation. In [2] and [12], the preconditioners were constructed based on the Laplacian. To make the preconditioner more efficient, [19] used the Laplacian perturbed by a real-valued linear term as a preconditioner. This kind of preconditioner is called the shifted Laplacian preconditioner, which is easy to construct. [9] proposed the preconditioner by perturbing the Laplacian with a purely imaginary linear term. The work was generalized in [10] by making use of a complex-valued linear term to perturb the Laplacian, which leaded to a better preconditioner than by using a real-valued or a purely imaginary one. It can be considered as a complex shifted Laplacian preconditioner. The complex shifted Laplacian preconditioner is more favorable for the convergence of preconditioned Krylov subspace methods and attracts a lot of interest. The spectrum of the discrete Helmholtz operator preconditioned with a shifted Laplacian was analyzed in [30]. A comparison was made between the multigrid and incomplete LU shifted-Laplacian preconditioners in [11]. The complex shifted Laplacian preconditioner was extended to a parallel case in [20]. In [28], the shifted Laplacian preconditioner was tested with a fourth-order discretization of the Helmholtz operator. The positive stable preconditioner proposed in [35] is also based on a complex shifted Laplacian preconditioner.

For the preconditioned Krylov subspace method, it is required to invert the preconditioner. In practice, it is not necessary to obtain the exact inverse, and an approximate inverse is enough. Of course, the preconditioned Krylov subspace method will gain a more satisfactory convergence when the inverse of the preconditioner is approached more exactly. We should try to invert the preconditioner approximately at a lower cost. For this purpose, the multigrid method is a good choice [5, 32]. For multigrid, interpolation operator is a very important component, a good interpolation operator will improve the robustness and efficiency of the multigrid method. The classic bilinear interpolation gives satisfactory convergence results for constant coefficients and mildly varying wavenumbers, but it is not robust enough for the case of highly variable coefficients and high wavenumbers. In [10], a multigrid method based on Zeeuw's interpolation operator [8] was used to approximately invert the preconditioner, and the interpolation operator showed a good performance.

In this paper, to solve the Helmholtz-PML equation, we generalize the complex shifted Laplacian preconditioner to the complex shifted Laplacian-PML preconditioner. Since the spectrum governs the convergence of iterative methods, a spectral analysis is important. We specially analyze the spectral distribution of the linear system discretized from the Helmholtz-PML equation preconditioned with a complex shifted Laplacian-PML by an optimal 9-point difference scheme. A clustered spectrum, which favors the convergence of Krylov subspace method, is presented. It is approximately moon-shaped, which differs from the curved spectrum in [10]. We illustrate the approximately moon-shaped spectrum which is enclosed by certain circle from the perspective of linear fractional map in complex variable function, which is also somewhat different from the results in [10]. We also make a series of numerical experiments which help to prove numerically that there holds the condition for the spectrum being enclosed by certain circle. After the spectral analysis, we propose a new matrix-based multigrid according to [8,22]. The interpolation in [8] was specially proposed for the convection–diffusion problems, while the one in [22] has complex coefficients, which works poorly for our problems. In this paper, a new interpolation operator is designed properly according to the situation we are considering. The new interpolation operator is contributed by a nearly symmetric matrix, and it takes into account the influence of the Helmholtz zeroth-order term for the construction of interpolation, which differs from the one in [10]. The corresponding multigrid is called a black-box multigrid as the interpolation operator can be computed in a black-box way. Since the success of multigrid is determined by a perfect interplay between smoothing and coarse-grid correction, we use a Local Fourier Analysis (LFA) tool [24,26,33,34] to see the smoothing properties of the Jacobi smoother for PML and the coarse-grid correction process. For computation, we adopt the Bi-CGSTAB, and use the black-box multigrid with newly proposed interpolation operator to invert the preconditioner approximately. Numerical experiments are given to illustrate the efficiency of preconditioned Bi-CGSTAB with black-box multigrid. In the experiments, the wavenumber value ranges from constant to greatly varying ones (the salt dome model). For the case of constant wavenumber, the value of dimensionless wavenumber [16] is as large as 900. The numerical experiments illustrate the robustness and efficiency of the preconditioned Bi-CGSTAB with the multigrid based on new interpolation operator, and it is more pronounced for greatly varying wavenumbers and large constant wavenumbers. We also have compared the performance of the new interpolation operator with the classic bilinear interpolation operator and the one proposed in [10]. The numerical results show that the newly proposed interpolation operator outperforms both the classic bilinear interpolation operator and the one suggested in [10].

This paper is organized as follows. In Section 2, the complex shifted Laplacian preconditioner for Helmholtz-PML equation will be discussed firstly, then a spectral analysis is presented for the discrete Helmholtz-PML operator preconditioned with a complex shifted Laplacian-PML. In Section 3, we propose a new interpolation operator for the black-box multigrid, and describe the preconditioned Bi-CGSTAB method with the black-box multigrid. In Section 4, numerical experiments are

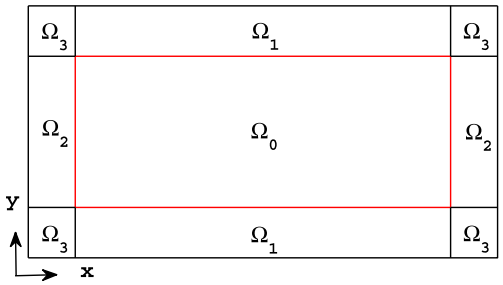

Fig. 1. The perfectly matched layer.

presented to confirm the efficiency of the preconditioned Bi-CGSTAB. The first example is about the constant wavenumbers, whereas the last two correspond to the varying wavenumbers. Finally, in Section 5, some conclusions are drawn.

2. Spectral analysis for the discrete Helmholtz-PML operator preconditioned with a complex shifted Laplacian-PML

In this section we develop the complex shifted Laplacian-PML preconditioner for the Helmholtz-PML equation, and analyze the spectral distribution of the discrete preconditioned Helmholtz-PML operator.

2.1. A complex shifted Laplacian-PML preconditioner

Consider the Helmholtz equation for wave problems

$$\mathscr{A}u := -\Delta u - (1-\alpha i)k^2 u = g \quad \text{in } \mathbb{R}^2, \tag{2.1}$$

where $\Delta := \frac{\partial^2}{\partial x^2} + \frac{\partial^2}{\partial y^2}$ is the Laplacian, $i := \sqrt{-1}$ is the imaginary unit, α is the real number indicating the damping in the medium, k is the wavenumber defined as $k := 2\pi f/v$ with f indicating the frequency and v indicating the speed, g represents the source term, and u usually represents a pressure field which is the unknown to be determined. The wavenumber k is a constant for the homogeneous medium, and varies for the heterogeneous medium. In geophysical application, $0 \leqslant \alpha \ll 1$, and can be set up to 5% ($i.e., \alpha = 0.05$).

We apply PML technique to truncate the infinite domain of Eq. (2.1) into a bounded domain, and achieve the Helmholtz-PML equation (cf. [23])

$$\mathcal{A}u := -\frac{\partial}{\partial x}\left(\frac{e_y}{e_x}\frac{\partial u}{\partial x}\right) - \frac{\partial}{\partial y}\left(\frac{e_x}{e_y}\frac{\partial u}{\partial y}\right) - (1-\alpha i)e_x e_y k^2 u = g \tag{2.2}$$

or its simplified form (cf. [27])

$$-\frac{1}{e_x^2}\frac{\partial^2 u}{\partial x^2} - \frac{1}{e_y^2}\frac{\partial^2 u}{\partial y^2} - (1-\alpha i)k^2 u = g, \tag{2.3}$$

where $e_x := 1 - i\frac{\sigma_x}{\omega}$ and $e_y := 1 - i\frac{\sigma_y}{\omega}$, in which $\omega := 2\pi f$ is the angular frequency, σ_x is a function only of x defined as

$$\sigma_x := \begin{cases} 2\pi a_0 f_0 (\frac{l_x}{L_{\mathrm{PML}}})^2, & \text{inside PML}, \\ 0, & \text{outside PML}, \end{cases} \tag{2.4}$$

and σ_y is defined similarly. Here, f_0 is the dominant frequency of the source, L_{PML} is the thickness of PML, l_x is the distance from interface between the interior region and PML region, and a_0 is a constant. We shall choose $a_0 = 1.79$ in our computation according to [23]. The wavelength is defined by $\iota := v/f$, the number of wavelengths in a square domain of size H equals H/ι. The dimensionless wavenumber is $2\pi f H/v$. In the remaining of the text, the wavenumber refers to dimensionless wavenumber, which is also denoted by k. The thickness of PML is chosen to be a half-wavelength or so, and the reflection will be tiny in practice. For a rectangular domain, its PML can be constructed as Fig. 1. The domain Ω_0 is the interested domain, while Ω_1, Ω_2, Ω_3 are the domains of PML. There holds that $\sigma_x \equiv \sigma_y \equiv 0$ in Ω_0, $\sigma_x \equiv 0$ in Ω_1 and $\sigma_y \equiv 0$ in Ω_2. In the corner domain Ω_3, $\sigma_x \neq 0$, $\sigma_y \neq 0$.

Applying a difference scheme to discretize (2.2), we obtain a linear system of the form

$$\mathbf{A}\mathbf{u} = \mathbf{g}, \tag{2.5}$$

where $\mathbf{A} \in \mathbb{C}^{N\times N}$, $\mathbf{u}, \mathbf{g} \in \mathbb{C}^N$, $\mathbb{C}$ is the complex number set and N is the number of unknowns. The matrix $\mathbf{A}$ has the form

$$\mathbf{A} := \mathbf{L} - z_1\mathbf{D}, \tag{2.6}$$

where $z_1 := 1-\alpha i$ and, $\mathbf{L}$, $\mathbf{D}$ are discretizations of the Laplacian-PML $-\frac{\partial}{\partial x}(\frac{e_y}{e_x}\frac{\partial}{\partial x})-\frac{\partial}{\partial y}(\frac{e_x}{e_y}\frac{\partial}{\partial y})$ and the operator corresponding to the zeroth-order term $e_x e_y k^2$, respectively. Moreover, $\mathbf{A}$ has complex entries, and is sparse, diagonal-distributional and nearly symmetric.

To make the Krylov subspace method competitive for solving the linear system (2.5), it is often preferable to solve the preconditioned linear system

$$\mathbf{M}^{-1}\mathbf{A}\mathbf{u} = \mathbf{M}^{-1}\mathbf{g}, \tag{2.7}$$

or

$$\mathbf{A}\mathbf{M}^{-1}\mathbf{v} = \mathbf{g}, \qquad \mathbf{v} = \mathbf{M}\mathbf{u}, \tag{2.8}$$

where $\mathbf{M}$, called the preconditioner, is a non-singular matrix. The choice of the preconditioner $\mathbf{M}$ is important in actual implementations. A good preconditioner is usually chosen such that the coefficient matrix of preconditioned system has a favorable spectral distribution so that the condition number is lower and the iterative method has a fast convergence. An efficient preconditioner should also be cheap to construct and make the preconditioned system easy to be solved [4].

For the Helmholtz equation (2.1), some preconditioners are based on the operator

$$\mathscr{M} := -\Delta - (\beta_1 - \beta_2 i)k^2. \tag{2.9}$$

For $(\beta_1,\beta_2) = (0,0)$, it is the Laplacian preconditioner presented in [12]. Preconditioners proposed in [19] and [9] correspond to $(\beta_1,\beta_2) = (-1,0)$ and $(\beta_1,\beta_2) = (0,1)$ respectively. For $\beta_1 > 0$ and $\beta_2 > 0$, it is the complex shifted Laplacian preconditioner studied in [10]. The complex shifted Laplacian preconditioner is an improved preconditioner, which is more favorable for the convergence of preconditioned Krylov subspace methods. It is easy to observe that the operator $\mathscr{M}$ just differs from $\mathscr{A}$ a little, and $\mathscr{M} = \mathscr{A}$ if $\beta_1 = 1$ and $\beta_2 = \alpha$. As is known, the multigrid method for the discrete Helmholtz equation diverges with increasing wavenumbers. However, the multigrid method for the linear system stemming from $\mathscr{M}$ shall converge for certain choice of β_1 and β_2, especially β_2 (see [18]). Generally, β_1 is chosen to be one. However, the value of β_2 has to be chosen properly in order to achieve a faster convergence for preconditioned Krylov subspace methods. It should be neither too large nor too small, otherwise, it will weaken the efficiency of preconditioned Krylov subspace methods. In [10], the authors suggested that the value of β_2 could be chosen by experience according to the relaxation factor of pointwise Jacobi iteration. $(\beta_1,\beta_2) = (1,1)$ was considered to be a basic parameter choice, and $(\beta_1,\beta_2) = (1,0.5)$, $(\beta_1,\beta_2) = (1,0.3)$ were two more advanced parameter choices.

In this paper, for the Helmholtz-PML equation (2.2), the preconditioner we consider is based on the operator

$$\mathcal{M} := -\frac{\partial}{\partial x}\left(\frac{e_y}{e_x}\frac{\partial u}{\partial x}\right) - \frac{\partial}{\partial y}\left(\frac{e_x}{e_y}\frac{\partial u}{\partial y}\right) - (\beta_1 - \beta_2 i)e_x e_y k^2. \tag{2.10}$$

If $\beta_1, \beta_2 > 0$, we name the operator (2.10) as the complex shifted Laplacian-PML preconditioner. As can be seen, when $e_x = e_y = 1$, (2.10) is equivalent to operator (2.9). The complex shifted Laplacian-PML preconditioner will also give a clustered spectrum, which is shaped approximately like a moon, while the complex shifted Laplacian preconditioner in [10] gives a clustered spectrum, which is a curved shape. In practice, we choose $\beta_1 = 1$ in (2.10). As to the choice of β_2, a test is done, and a table is given in Section 4.1, which shows the effect of different parameter choices on the convergence of the multigrid method and the Bi-CGSTAB method. Combining numerical experiments shown in Table 4 and the suggestion in [10], we choose $(\beta_1,\beta_2) = (1,0.5)$ as a basic parameter choice.

Now, we use operator (2.10) to precondition the Helmholtz-PML equation (2.2). The preconditioned equation in the operator form can be written as

$$\mathcal{A}\mathcal{M}^{-1}v = g, \qquad v = \mathcal{M}u. \tag{2.11}$$

Applying the same difference scheme to discretize $\mathcal{M}$, we obtain the preconditioner $\mathbf{M}$ and preconditioned system

$$\mathbf{A}\mathbf{M}^{-1}\mathbf{v} = \mathbf{g}, \qquad \mathbf{v} = \mathbf{M}\mathbf{u}, \tag{2.12}$$

where

$$\mathbf{M} := \mathbf{L} - z_2\mathbf{D}, \qquad z_2 := \beta_1 - \beta_2 i. \tag{2.13}$$

As can be seen, $\mathbf{M}$ can be constructed easily.

2.2. Spectral analysis of the discrete preconditioned Helmholtz-PML operator

We now study the spectral distribution of the discrete preconditioned Helmholtz-PML operator. Similar analysis was given by [30] for the discrete Helmholtz operator, with the homogeneous Neumann condition, homogeneous Dirichlet condition and Sommerfeld condition, preconditioned with a shifted Laplacian.

We start with the concept of generalized eigenvalues. For any matrices $\mathbf{A}, \mathbf{B} \in \mathbb{C}^{N\times N}$ the (generalized) eigenvalues of $\mathbf{A}$ with respect to $\mathbf{B}$ are the roots of the equation $\det(\mathbf{A} - \lambda\mathbf{B}) = 0$. The set of all eigenvalues of $\mathbf{A}$ with respect to $\mathbf{B}$ is denoted by $\sigma(\mathbf{A},\mathbf{B})$, which is called the spectrum of $\mathbf{A}$ with respect to $\mathbf{B}$. If $\lambda \in \sigma(\mathbf{A},\mathbf{B})$ and $\mathbf{x} \in \mathbb{C}^N$ satisfy

$$\mathbf{A}\mathbf{x} = \lambda\mathbf{B}\mathbf{x}, \qquad \mathbf{x} \neq 0$$

then $\mathbf{x}$ is called the generalized eigenvector of $\mathbf{A}$ with respect to $\mathbf{B}$. When $\mathbf{B}$ is the identity matrix $\mathbf{I}$, we denote $\sigma(\mathbf{A}) := \sigma(\mathbf{A}, \mathbf{I})$. It is clear that $\sigma(\mathbf{A}\mathbf{M}^{-1}) = \sigma(\mathbf{M}^{-1}\mathbf{A}) = \sigma(\mathbf{A}, \mathbf{M})$ if $\mathbf{M} \in \mathbb{C}^{N\times N}$ is nonsingular.

We introduce a useful lemma for our spectral analysis, which is a slight generalization of the similar result described in [30] with a different presentation.

Lemma 2.1. *Let $\mathbf{L}, \mathbf{D} \in \mathbb{C}^{N\times N}$, $\mathbf{A} := \mathbf{L} - z_1\mathbf{D}$ and $\mathbf{M} := \mathbf{L} - z_2\mathbf{D}$ with $z_1, z_2 \in \mathbb{C}$. If $\mathbf{D}$ and $\mathbf{M}$ are nonsingular, $\mu \in \mathbb{C}$ and $\lambda := \frac{\mu - z_1}{\mu - z_2}$ with $\mu \neq z_2$ then $\lambda \in \sigma(\mathbf{A}, \mathbf{M})$ if and only if $\mu \in \sigma(\mathbf{L}, \mathbf{D})$, and $\mathbf{M}^{-1}\mathbf{A}$, $\mathbf{D}^{-1}\mathbf{L}$ share the same eigenvectors.*

Proof. If $\mu \in \sigma(\mathbf{L}, \mathbf{D})$ then we have $\mathbf{x} \neq 0$ such that

$$\mathbf{L}\mathbf{x} = \mu\mathbf{D}\mathbf{x},$$

which leads to that

$$\mathbf{A}\mathbf{x} = (\mathbf{L} - z_1\mathbf{D})\mathbf{x} = (\mu - z_1)\mathbf{D}\mathbf{x},$$

and

$$\mathbf{M}\mathbf{x} = (\mathbf{L} - z_2\mathbf{D})\mathbf{x} = (\mu - z_2)\mathbf{D}\mathbf{x}.$$

Therefore,

$$\mathbf{A}\mathbf{x} = \frac{\mu - z_1}{\mu - z_2}\mathbf{M}\mathbf{x} = \lambda\mathbf{M}\mathbf{x},$$

which means $\lambda \in \sigma(\mathbf{A}, \mathbf{M})$. Conversely, if $\lambda \in \sigma(\mathbf{A}, \mathbf{M})$, then we have $\mathbf{x} \neq 0$ such that

$$\mathbf{A}\mathbf{x} = \lambda\mathbf{M}\mathbf{x},$$

that is,

$$(\mathbf{L} - z_1\mathbf{D})\mathbf{x} = \frac{\mu - z_1}{\mu - z_2}(\mathbf{L} - z_2\mathbf{D})\mathbf{x}.$$

A simple computation yields

$$\mathbf{L}\mathbf{x} = \mu\mathbf{D}\mathbf{x}.$$

This means $\mu \in \sigma(\mathbf{L}, \mathbf{D})$ and completes the proof. □

According to Lemma 2.1, in order to locate the eigenvalues λ of the discrete preconditioned Helmholtz-PML operator $\mathbf{A}\mathbf{M}^{-1}$, we have to learn about the location of eigenvalues μ for $\mathbf{D}^{-1}\mathbf{L}$. Noting that the mapping $\lambda : \mathbb{C} \to \mathbb{C}$ defined by

$$\lambda = \lambda(\mu) := \frac{\mu - z_1}{\mu - z_2} \tag{2.14}$$

is a linear fractional map on the extended complex plane, and relevant to this we have the following lemma. For the description, we denote the real and imaginary parts of μ by $\mathrm{Re}(\mu)$ and $\mathrm{Im}(\mu)$ respectively.

Lemma 2.2. *The linear fractional mapping $\lambda : \mathbb{C} \to \mathbb{C}$ defined by* (2.14) *maps the real axis (i.e., $\mu - \bar{\mu} = 0$) to the circle with center $c := \frac{z_1 - \bar{z}_2}{z_2 - \bar{z}_2}$ and radius $R := |\frac{z_2 - z_1}{z_2 - \bar{z}_2}|$, denoted by $O(c, R)$. Moreover, $\lambda(\mu)$ with $\mathrm{Im}(\mu) = 0$ is on $O(c, R)$, $\lambda(\mu)$ with $\mathrm{Im}(\mu) > 0$ is inside $O(c, R)$, and $\lambda(\mu)$ with $\mathrm{Im}(\mu) < 0$ is outside $O(c, R)$.*

Proof. In the complex plane $\mathbb{C} = \{\mu:\ \mu = x + yi,\ x, y \in \mathbb{R}\}$, a circle can be represented by

$$A\left(x^2 + y^2\right) + Bx + Cy + D = 0 \tag{2.15}$$

with parameters $A, B, C, D \in \mathbb{R}$ satisfying $B^2 + C^2 > 4AD$. The center of this circle is $(\frac{B}{2A}, \frac{C}{2A})$ and the radius is $R := \frac{\sqrt{B^2 + C^2 - 4AD}}{2A}$. Noting that

$$x = \frac{\mu + \bar{\mu}}{2}, \qquad y = \frac{\mu - \bar{\mu}}{2i}, \qquad x^2 + y^2 = \mu\bar{\mu},$$

(2.15) can be rewritten as

$$A\mu\bar{\mu} + E\bar{\mu} + \bar{E}\mu + D = 0 \tag{2.16}$$

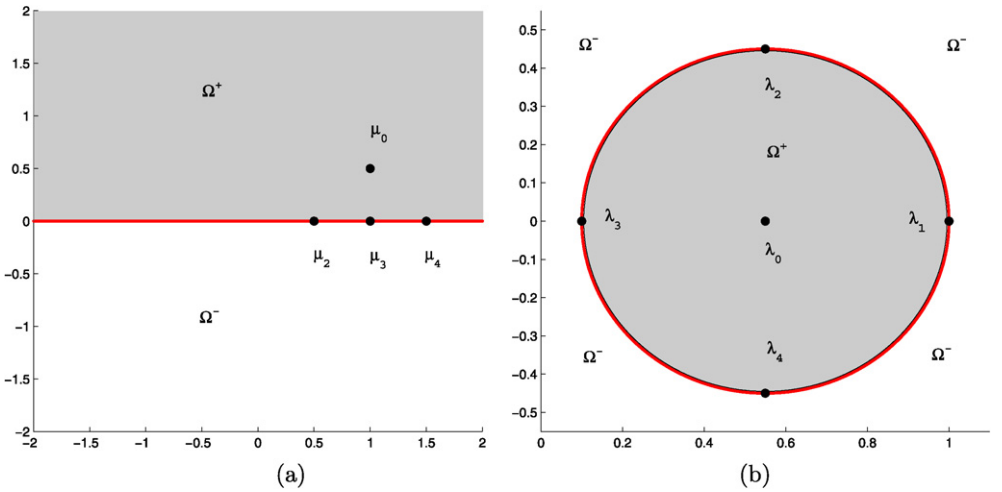

Fig. 2. The linear fractional map. (For interpretation of colors in this figure, the reader is referred to the web version of this article.)

with $E := \frac{1}{2}(B + Ci)$, $|E|^2 > AD$. The center and the radius can be represented by $c = -\frac{E}{A}$ and $R = \frac{\sqrt{|E|^2 - AD}}{A}$ respectively. When $A = 0$, (2.16) represents a straight line which can be considered as the circle with $R = \infty$. The real axis is represented by

$$\mu - \bar{\mu} = 0. \tag{2.17}$$

From (2.14), we have

$$\mu = \frac{z_2\lambda - z_1}{\lambda - 1}, \qquad \bar{\mu} = \frac{\bar{z}_2\bar{\lambda} - \bar{z}_1}{\bar{\lambda} - 1}. \tag{2.18}$$

Substitution of (2.18) into (2.17) yields

$$A'\lambda\bar{\lambda} + E'\bar{\lambda} + \bar{E}'\lambda + D' = 0, \tag{2.19}$$

where $A' := (z_2 - \bar{z}_2)i$, $E' := (\bar{z}_2 - z_1)i$ and $D' := (\bar{z}_2 - \bar{z}_1)i$. Thus, (2.19) represents a circle, denoted by $O(c, R)$, with the center $c := -\frac{E'}{A'} = \frac{z_1 - \bar{z}_2}{z_2 - \bar{z}_2}$ and the radius $R := \frac{\sqrt{|E'|^2 - A'D'}}{A'} = |\frac{z_2 - z_1}{z_2 - \bar{z}_2}|$. This means that μ with $\mathrm{Im}(u) = 0$ is mapped into the circle $O(c, R)$. It can be easily seen that μ with $\mathrm{Im}(u) > 0$ is mapped inside $O(c, R)$, and μ with $\mathrm{Im}(u) < 0$ is mapped outside $O(c, R)$. □

With the help of Lemma 2.2 we have the following proposition.

Proposition 2.3. *Let the linear fractional mapping $\lambda : \mathbb{C} \to \mathbb{C}$ be defined by* (2.14) *with $z_1 := 1 - \alpha i$, $z_2 := 1 - \beta i$ and $\beta > \alpha \geqslant 0$. Then the real axis (i.e., $\mu - \bar{\mu} = 0$) is mapped to the circle $O(c, R)$ with $c := \frac{\beta + \alpha}{2\beta}$ and $R := \frac{\beta - \alpha}{2\beta}$, the upper half-plane is mapped inside $O(c, R)$, and the lower half-plane is mapped outside of $O(c, R)$. Let $l := \inf_{\mu \in O(c,R)} |\mu|$ being the distance between the origin and $O(c, R)$, then we have $l = \frac{\alpha}{\beta}$.*

Proof. The results of this proposition follow from Lemma 2.2 with $z_1 := 1 - \alpha i$ and $z_2 := 1 - \beta i$. □

Fig. 2 presents the linear fractional map (2.14) with $\alpha = 0.05$, $\beta_1 = 1$ and $\beta_2 = \beta = 0.5$. In Fig. 2(a), the extended complex plane $\mathbb{C}$ is divided into three parts: the upper half-plane (the shadow region, denoted by Ω^+), the real axis (red line), and the lower half-plane (Ω^-). It is observed that the real axis is mapped to the circle with center $c = 0.55$, $R = 0.45$, and Ω^+, Ω^- are mapped inside and outside of the circle respectively. Moreover, the points $\mu_0 = 1 + \beta i$, $\mu_1 = \infty$, $\mu_2 = 1 - \beta$, $\mu_3 = 1$, $\mu_4 = 1 + \beta$ in Fig. 2(a) are mapped to $\lambda_0 = c = \frac{\beta + \alpha}{2\beta}$, $\lambda_1 = 1$, $\lambda_2 = \frac{\beta + \alpha}{2\beta} + \frac{\beta - \alpha}{2\beta} i$, $\lambda_3 = \frac{\alpha}{\beta}$, $\lambda_4 = \frac{\beta + \alpha}{2\beta} - \frac{\beta - \alpha}{2\beta} i$ in Fig. 2(b), respectively.

For any matrix $\mathbf{E}$, we denote $\mathrm{Re}(\mathbf{E})$ and $\mathrm{Im}(\mathbf{E})$ the real and imaginary parts of $\mathbf{E}$ respectively. When $\mathbf{E}$ is real, we denote $\mu(\mathbf{E})_{\min}$ and $\mu(\mathbf{E})_{\max}$ the smallest and the largest eigenvalues of $\mathbf{E}$ respectively. To provide the following lemma, we recall the Bendixon theorem (cf. [15]) that for any matrix $\mathbf{E}$,

$$\mu\big(\mathrm{Re}(\mathbf{E})\big)_{\min} \leqslant \mathrm{Re}\big(\mu(\mathbf{E})\big) \leqslant \mu\big(\mathrm{Re}(\mathbf{E})\big)_{\max},$$

and

$$\mu\big(\mathrm{Im}(\mathbf{E})\big)_{\min} \leqslant \mathrm{Im}\big(\mu(\mathbf{E})\big) \leqslant \mu\big(\mathrm{Im}(\mathbf{E})\big)_{\max}. \tag{2.20}$$

Lemma 2.4. *Let* $\mathbf{L}$ *be complex symmetric matrix and* $\mathbf{D}$ *be real symmetric matrix. If* $\mathrm{Im}(\mathbf{L})$ *is positive semidefinite and* $\mathbf{D}$ *is positive definite, then the eigenvalues* $\mu \in \sigma(\mathbf{L}, \mathbf{D})$ *have a nonnegative imaginary part, that is,* $\mathrm{Im}(\mu) \geqslant 0$.

Proof. It follows from $\mu \in \sigma(\mathbf{L}, \mathbf{D})$ that there exists $\mathbf{x} \neq 0$ such that

$$\mathbf{L}\mathbf{x} = \mu \mathbf{D}\mathbf{x}.$$

Since $\mathbf{D}$ is real symmetric positive definite, there is a nonsingular real symmetric matrix $\mathbf{U}$ such that $\mathbf{D} = \mathbf{U}^2$. Therefore, we have that

$$\mathbf{U}^{-1}\mathbf{L}\mathbf{U}^{-1}\mathbf{y} = \mu \mathbf{y}, \tag{2.21}$$

where $\mathbf{y} = \mathbf{U}\mathbf{x} \neq 0$. Using (2.20) with $\mathbf{E} = \mathbf{U}^{-1}\mathbf{L}\mathbf{U}^{-1}$, and noting that $\mathrm{Im}(\mathbf{E})$ is symmetric positive semidefinite, we conclude

$$\mathrm{Im}\big(\mu(\mathbf{E})\big) \geqslant \mu\big(\mathrm{Im}(\mathbf{E})\big)_{\min} > 0.$$

This completes the proof. □

The following proposition follows immediately from Proposition 2.3 and Lemma 2.4.

Proposition 2.5. *Suppose that* $\mathbf{L}$ *is complex symmetric matrix, its imaginary part* $\mathrm{Im}(\mathbf{L})$ *is positive semidefinite, and* $\mathbf{D}$ *is a symmetric positive definite matrix. If* $z_1 := 1 - \alpha i$ *and* $z_2 := 1 - \beta i$ *with* $\beta > \alpha \geqslant 0$, *then the eigenvalues* $\lambda \in \sigma(\mathbf{A}, \mathbf{M})$ *are enclosed by the circle* $O(\frac{\beta+\alpha}{2\beta}, \frac{\beta-\alpha i}{2\beta})$.

In Proposition 2.5, we obtain that $\lambda \in \sigma(\mathbf{A}, \mathbf{M})$ are enclosed by some circle under certain conditions from the perspective of linear fractional map in complex variable function, which is somewhat different from the results in [30].

We now turn our attention to the discrete Helmholtz-PML operator. We discretize Eq. (2.2) by using an optimal 9-point difference scheme proposed in [6].

In [6], we had investigated the rotated 9-point finite difference scheme and showed that it was not pointwise consistent with the Helmholtz-PML equation. Then, we presented an optimal 9-point difference scheme, which was consistent with the Helmholtz-PML equation, and also a second-order scheme. We then proposed global and refined choice strategies for choosing optimal parameters of the 9-point finite difference scheme based on minimizing the numerical dispersion. Compared with the rotated 9-point finite difference scheme (cf. [17]), the optimal 9-point finite difference method proposed in [6] behaves much better with respect to k. In [6], we consider a problem which was used for measuring the efficiency of numerical methods in [1], and numerical results illustrate the improvement of the accuracy and the reduction of the numerical dispersion. Especially for large wavenumbers, the improvement is more pronounced. In some sense, the new optimal 9-point finite-difference stencil suppresses the "pollution effect" of large wavenumbers. The largest wavenumber considered in [6] is $k = 500$.

The stencil notation at (x_m, y_n) is denoted by

$$\begin{bmatrix} b_7 & b_8 & b_9 \\ b_4 & b_5 & b_6 \\ b_1 & b_2 & b_3 \end{bmatrix}, \tag{2.22}$$

where the entries are given by

$$\begin{aligned}
b_1 &:= \frac{1-b}{2h^2}(A_{m-\frac{1}{2},n-1} + B_{m-1,n-\frac{1}{2}}) + \frac{e}{4}k^2 C_{m-1,n-1},\\
b_2 &:= -\frac{1-b}{2h^2}(A_{m+\frac{1}{2},n-1} + A_{m-\frac{1}{2},n-1}) + \frac{b}{h^2}B_{m,n-\frac{1}{2}} + \frac{d}{4}k^2 C_{m,n-1},\\
b_3 &:= \frac{1-b}{2h^2}(A_{m+\frac{1}{2},n-1} + B_{m+1,n-\frac{1}{2}}) + \frac{e}{4}k^2 C_{m+1,n-1},\\
b_4 &:= -\frac{1-b}{2h^2}(B_{m-1,n+\frac{1}{2}} + B_{m-1,n-\frac{1}{2}}) + \frac{b}{h^2}A_{m-\frac{1}{2},n} + \frac{d}{4}k^2 C_{m-1,n},\\
b_5 &:= -\frac{b}{h^2}(A_{m+\frac{1}{2},n} + A_{m-\frac{1}{2},n} + B_{m,n+\frac{1}{2}} + B_{m,n-\frac{1}{2}}) + (1-d-e)k^2 C_{m,n},\\
b_6 &:= -\frac{1-b}{2h^2}(B_{m+1,n+\frac{1}{2}} + B_{m+1,n-\frac{1}{2}}) + \frac{b}{h^2}A_{m+\frac{1}{2},n} + \frac{d}{4}k^2 C_{m+1,n},\\
b_7 &:= \frac{1-b}{2h^2}(A_{m-\frac{1}{2},n+1} + B_{m-1,n+\frac{1}{2}}) + \frac{e}{4}k^2 C_{m-1,n+1},\\
b_8 &:= -\frac{1-b}{2h^2}(A_{m+\frac{1}{2},n+1} + A_{m-\frac{1}{2},n+1}) + \frac{b}{h^2}B_{m,n+\frac{1}{2}} + \frac{d}{4}k^2 C_{m,n+1},\\
b_9 &:= \frac{1-b}{2h^2}(A_{m+\frac{1}{2},n+1} + B_{m+1,n+\frac{1}{2}}) + \frac{e}{4}k^2 C_{m+1,n+1},
\end{aligned}$$

in which h is the discretization step, $b, d, e \in \mathbb{R}$ are parameters optimized by global and refined choice strategies based on minimizing the numerical dispersion (see [6]), and $A_{m+\frac{i}{2},n+\frac{j}{2}}$, $B_{m+\frac{i}{2},n+\frac{j}{2}}$ and $C_{m,n}$ are defined as

$$A_{m+\frac{i}{2},n+\frac{j}{2}} := A\left(x_0 + \left(m-1+\frac{i}{2}\right)h,\, y_0 + \left(n-1+\frac{j}{2}\right)h\right),$$
$$B_{m+\frac{i}{2},n+\frac{j}{2}} := B\left(x_0 + \left(m-1+\frac{i}{2}\right)h,\, y_0 + \left(n-1+\frac{j}{2}\right)h\right),$$
$$C_{m,n} := C\big(x_0 + (m-1)h,\, y_0 + (n-1)h\big)$$

for $i, j \in \mathbb{Z}_3 := \{-2, -1, 0, 1, 2\}$, with

$$A := \frac{e_y}{e_x}, \qquad B := \frac{e_x}{e_y}, \quad \text{and} \quad C := e_x e_y.$$

The discrete Helmholtz-PML operator obtained by the difference scheme does not satisfy the conditions of Proposition 2.5 due to the PML. In fact, $\mathbf{L}$ is a nearly symmetric matrix, $\mathrm{Re}(\mathbf{L})$, $\mathrm{Im}(\mathbf{L})$ are nearly positive semidefinite matrices, and $\mathbf{D}$ can be symmetric positive definite when a proper optimized coefficients are used. Therefore, we cannot directly obtain that the eigenvalues $\lambda \in \sigma(\mathbf{A}, \mathbf{M})$ are enclosed by certain circle, but we may expect that the eigenvalues are approximately enclosed by the circle $O(\frac{\beta+\alpha}{2\beta}, \frac{\beta-\alpha}{2\beta})$ since the effect of the PML on the whole symmetry is slight. To see this, we define a symmetric matrix

$$\tilde{\mathbf{L}} := \mathbf{F} + (\mathbf{G} + \mathbf{H})i,$$

where $\mathbf{F} := (\mathrm{Re}(\mathbf{L}) + \mathrm{Re}(\mathbf{L})^T)/2$, $\mathbf{G} := [g_{ij}]_{N\times N} = (\mathrm{Im}(\mathbf{L}) + \mathrm{Im}(\mathbf{L})^T)/2$, and $\mathbf{H}$ is a diagonal matrix defined as

$$\mathbf{H} := \mathrm{diag}\{h_1, \ldots, h_N\}, \quad \text{with } h_i := \left|\min\left\{g_{ii} - \sum_{j\neq i} |g_{ij}|, 0\right\}\right|, \quad i = 1, \ldots, N.$$

Let $\tilde{\mathbf{A}} := \tilde{\mathbf{L}} - z_1\mathbf{D}$ and $\tilde{\mathbf{M}} := \tilde{\mathbf{L}} - z_2\mathbf{D}$ with $z_1 := 1 - \alpha i$ and $z_2 := 1 - \beta i$. It is clear that $\tilde{\mathbf{L}}$ satisfies the conditions of Proposition 2.5, and

$$\|\mathbf{A} - \tilde{\mathbf{A}}\| = \|\mathbf{M} - \tilde{\mathbf{M}}\| = \|\mathbf{L} - \tilde{\mathbf{L}}\| = \left\|\frac{1}{2}\big(\mathbf{L} - \mathbf{L}^T\big) - \mathbf{H}i\right\| \leqslant \frac{1}{2}\big\|\big(\mathbf{L} - \mathbf{L}^T\big)\big\| + \|\mathbf{H}\|.$$

According to Lemma 2.4 and Proposition 2.5, $\tilde{\mu} \in \sigma(\tilde{\mathbf{L}}, \mathbf{D})$ have a nonnegative imaginary part, and $\tilde{\lambda} \in \sigma(\tilde{\mathbf{A}}, \tilde{\mathbf{M}})$ are enclosed by the circle $O(\frac{\beta+\alpha}{2\beta}, \frac{\beta-\alpha}{2\beta})$. When the PML is not too thick, the error $\|\mathbf{L} - \tilde{\mathbf{L}}\|$ is small, so that $\mathbf{L}$ can be considered as a small perturbation of $\tilde{\mathbf{L}}$. However, even though the perturbation is small, nothing can be said theoretically about how the spectrum will be under such a perturbation. We shall rely on some numerical observation.

Fig. 3 shows the spectral distribution of matrices $\tilde{\mathbf{A}}$, $\mathbf{D}^{-1}\tilde{\mathbf{L}}$, $\tilde{\mathbf{M}}^{-1}\tilde{\mathbf{A}}$, and their perturbations $\mathbf{A}$, $\mathbf{D}^{-1}\mathbf{L}$, $\mathbf{M}^{-1}\mathbf{A}$ when $h = 1/128$, $k = 100$, $z_1 = 1$ and $z_2 = 1 - 0.5i$. The thickness of the PML is 10, that is, the PML possesses 10 gridpoints in each direction. In this case, we have $\|\mathbf{L} - \mathbf{L}^T\| \leqslant 0.0042$, $\|\mathbf{G}\| \leqslant 0.0037$, $\|\mathbf{A} - \tilde{\mathbf{A}}\| \leqslant 0.0058$, where $\|\cdot\|$ refers to the Euclidean norm $\|\cdot\|_2$. Fig. 3(a) is the original spectrum for $\tilde{\mathbf{A}}$, which is scattered over both the left and right half-planes. It can be seen that the real part of the spectrum includes a part of the negative real axis with large values. However, after preconditioning, a clustered spectrum, approximately moon-shaped, is observed in Fig. 3(c), and all of the eigenvalues move to the right half-plane. Moreover, we find that the eigenvalues after preconditioning are located on or inside the circle (plotted with red) with center $c = (0.5, 0)$ and radius $R = 0.5$, which is coincident with Proposition 2.5. This is guaranteed by the fact that $\sigma(\tilde{\mathbf{L}}, \mathbf{D})$ have a nonnegative imaginary part, which is presented in Fig. 3(b). Fig. 3(d), (e) and (f) are the spectrum for $\mathbf{A}$, $\mathbf{D}^{-1}\mathbf{L}$ and $\mathbf{M}^{-1}\mathbf{A}$, which are the corresponding perturbation for (a), (b) and (c) respectively. We can see that $\sigma(\mathbf{A}, \mathbf{M})$ in Fig. 3(f) has the similar distribution with $\sigma(\tilde{\mathbf{A}}, \tilde{\mathbf{M}})$ in (c), and it is still enclosed by the same circle (plotted with red). Fig. 4 shows the corresponding spectrum with h, k, z_2 the same as Fig. 3, but $z_1 = 1 - 0.05i$, namely, with 5% damping in (2.3). It is observed that $\sigma(\tilde{\mathbf{A}}, \tilde{\mathbf{M}})$ and its perturbation $\sigma(\mathbf{A}, \mathbf{M})$ are enclosed by the same circle with center $c = (0.55, 0)$ and radius $R = 0.45$. The circle is far away from the origin with a smaller radius due to $\alpha = 0.05 > 0$ according to Proposition 2.5.

It is commonly accepted that the Krylov subspace method would converge faster if the coefficient matrix has a more clustered spectrum away from the origin towards the right half-plane. The distribution of eigenvalues in Fig. 3(a), (d) and Fig. 4(a), (d) are not favorable for the Krylov subspace methods, and results in a very slow convergence or divergence. However, from Fig. 3(c), (f) and Fig. 4(c), (f), we can expect a faster convergence of Krylov subspace methods for the preconditioned systems. Fig. 4(c), (f) also indicates that the convergence of the Krylov subspace methods for the case with some damping will be faster than for the case without damping, since the spectrum of the damped ones move away farther from the origin than that of the undamped ones.

We estimate the location of $\sigma(\mathbf{A}, \mathbf{M})$ by considering it as a perturbation of $\sigma(\tilde{\mathbf{A}}, \tilde{\mathbf{M}})$ which is enclosed by a circle according to Proposition 2.5. Actually, Proposition 2.3 implies that $\lambda = \lambda(\mu) \in \sigma(\mathbf{A}, \mathbf{M})$ would be enclosed by some circle if $\mu \in \sigma(\mathbf{L}, \mathbf{D})$ has a nonnegative imaginary part. A series of numerical experiments show that we have $\mathrm{Im}(\mu) \geqslant 0$ indeed.

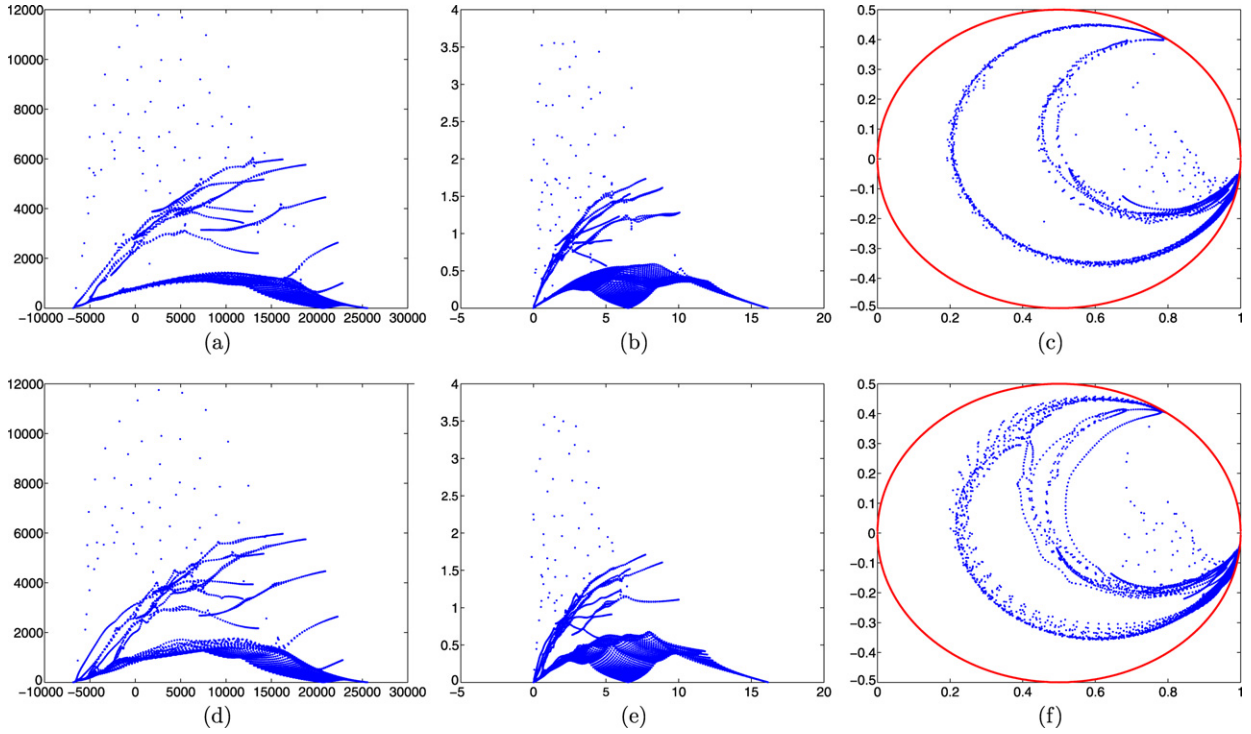

Fig. 3. The spectral distribution of the following matrices for $h = 1/128$, $k = 100$, $z_1 = 1$ and $z_2 = 1 - 0.5i$: (a) $\tilde{\mathbf{A}}$; (b) $\mathbf{D}^{-1}\tilde{\mathbf{L}}$; (c) $\tilde{\mathbf{M}}^{-1}\tilde{\mathbf{A}}$; (d) $\mathbf{A}$; (e) $\mathbf{D}^{-1}\mathbf{L}$; (f) $\mathbf{M}^{-1}\mathbf{A}$. (For interpretation of colors in this figure, the reader is referred to the web version of this article.)

In Tables 1, 2 and 3, the minimums of the imaginary parts of $\sigma(\mathbf{L})$ and $\sigma(\mathbf{L}, \mathbf{D})$ are presented with different wavenumbers k and different steps h. In the experiments, we choose the domain size $H = 1$, $kh \leqslant \frac{\pi}{4}$ for 8 points per wavelength, and denote

$$e_1 = \min\{\mathrm{Im}(\mu):\ \mu \in \sigma(\mathbf{L})\}, \qquad e_2 = \min\{\mathrm{Im}(\mu):\ \mu \in \sigma(\mathbf{L}, \mathbf{D})\}.$$

Tables 1, 2 and 3 correspond to $z_1 = 1$, $z_1 = 1 - 0.01i$, and $z_1 = 1 - 0.05i$ respectively. Due to the memory limitation, the largest wavenumber in the experiments is $k = 120$, and the corresponding matrix size is $154 \times 154 = 23\,716$. As can be seen from Tables 1, 2 and 3, all the minimums of imaginary parts of $\sigma(\mathbf{L})$ and $\sigma(\mathbf{L}, \mathbf{D})$ are positive for different k and h. Thus we can conclude that $\mu \in \sigma(\mathbf{L}, \mathbf{D})$ have a nonnegative imaginary part such that $\lambda \in \sigma(\mathbf{A}, \mathbf{M})$ are enclosed by the circle described in Propositions 2.3 and 2.5.

3. Preconditioned Bi-CGSTAB method with black-box multigrid

In this section, we present our algorithm for solving the Helmholtz-PML equation. The equation is preconditioned with a complex shifted Laplacian-PML and discretized by an optimal 9-point difference scheme as described in the last section. We shall combine the Bi-CGSTAB method (cf. [9]) and the black-box multigrid with a new interpolation operator to solve the resulting linear system (2.12).

First, we introduce the preconditioned Bi-CGSTAB algorithm for solving $\mathbf{Au} = \mathbf{g}$ with preconditioner $\mathbf{M}$.

Algorithm 3.1 *(Preconditioned Bi-CGSTAB method).*

1 $i \leftarrow 0$.
2 $\tilde{\mathbf{r}} \leftarrow 0$.
3 $\mathbf{u}^{(i)} \leftarrow 0$.
4 $\mathbf{r}^{(i)} \leftarrow \mathbf{g} - \mathbf{Au}^{(i)}$.
5 *While* $\frac{\|\mathbf{r}^{(i)}\|}{\|\mathbf{r}^{(0)}\|} > \epsilon$ (*Tolerance*)
6 $i \leftarrow i + 1$.
7 $\rho_{i-1} \leftarrow \tilde{\mathbf{r}}^T \mathbf{r}^{(i-1)}$.

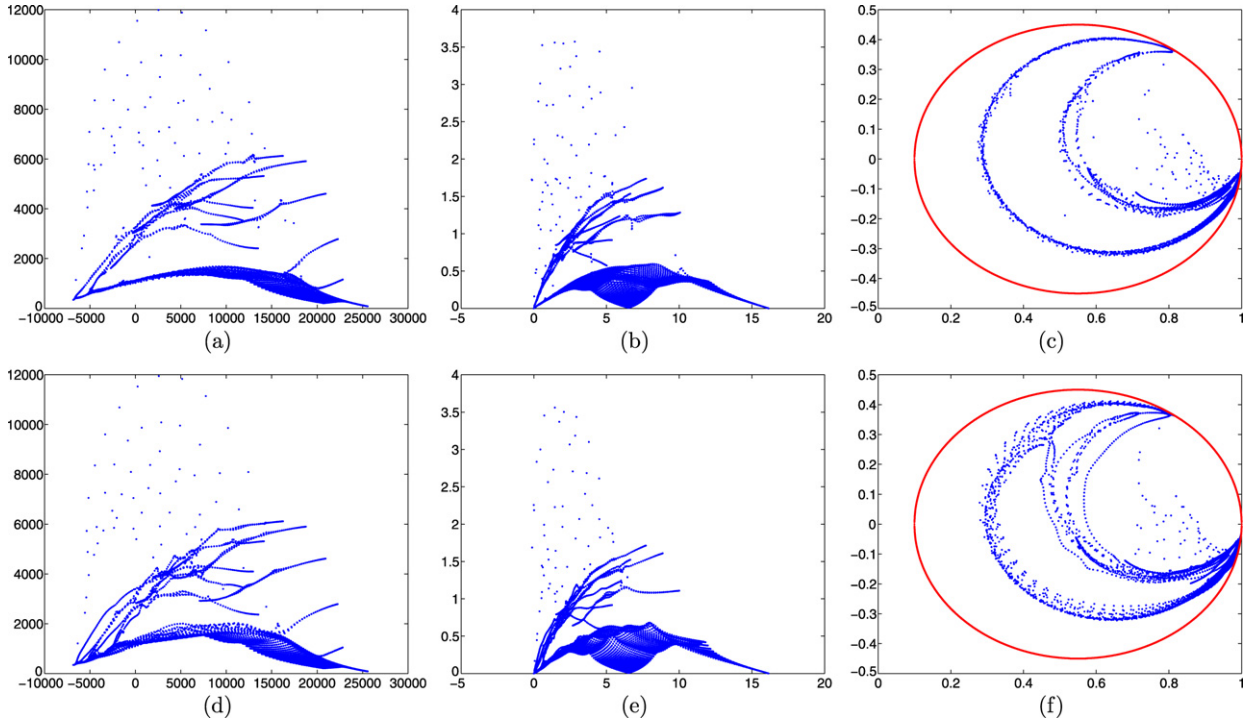

Fig. 4. The spectral distribution of the following matrices for $h = 1/128$, $k = 100$, $z_1 = 1 - 0.05i$ and $z_2 = 1 - 0.5i$: (a) $\tilde{\mathbf{A}}$; (b) $\mathbf{D}^{-1}\tilde{\mathbf{L}}$; (c) $\tilde{\mathbf{M}}^{-1}\tilde{\mathbf{A}}$; (d) $\mathbf{A}$; (e) $\mathbf{D}^{-1}\mathbf{L}$; (f) $\mathbf{M}^{-1}\mathbf{A}$.

Table 1
The minimum of the imaginary part of $\sigma(\mathbf{L})$, $\sigma(\mathbf{L}, \mathbf{D})$ for $z_1 = 1$.

k	40	50	60	70	80	90	100	110	120
h	1/51	1/64	1/77	1/90	1/102	1/115	1/128	1/141	1/153
e_1	8.07e−2	6.58e−2	5.55e−2	4.81e−2	4.36e−2	3.88e−2	1.16e−2	4.20e−3	1.68e−3
e_2	1.26e−4	5.57e−5	2.75e−5	1.49e−5	8.93e−6	5.42e−6	2.97e−6	1.78e−6	8.92e−7

Table 2
The minimum of the imaginary part of $\sigma(\mathbf{L})$, $\sigma(\mathbf{L}, \mathbf{D})$ for $z_1 = 1 - 0.01i$.

k	40	50	60	70	80	90	100	110	120
h	1/51	1/64	1/77	1/90	1/102	1/115	1/128	1/141	1/153
e_1	1.53e−1	1.40e−1	1.01e−1	7.43e−2	5.87e−2	4.55e−2	2.48e−2	9.00e−3	3.47e−3
e_2	1.27e−4	5.67e−5	2.79e−5	1.52e−5	9.17e−6	5.62e−6	3.00e−6	1.81e−6	9.01e−7

Table 3
The minimum of the imaginary part of $\sigma(\mathbf{L})$, $\sigma(\mathbf{L}, \mathbf{D})$ for $z_1 = 1 - 0.05i$.

k	40	50	60	70	80	90	100	110	120
h	1/51	1/64	1/77	1/90	1/102	1/115	1/128	1/141	1/153
e_1	2.07e−1	1.46e−1	1.06e−1	8.03e−2	6.51e−2	5.21e−2	2.57e−2	9.30e−3	3.57e−3
e_2	1.29e−4	5.82e−5	2.95e−5	1.63e−5	1.02e−5	6.43e−6	3.18e−6	2.04e−6	9.10e−7

8 *If* $\rho_{i-1} == 0$
9 *The method fails.*
10 *Else*
11 *If* $i == 1$
12 $\mathbf{p}^{(i)} \leftarrow \mathbf{r}^{(i-1)}$.
13 *Else*

$\beta_{i-1} \leftarrow \frac{\rho_{i-1}}{\rho_{i-2}} \cdot \frac{\alpha_{i-1}}{\omega_{i-1}}$.

$\mathbf{p}^{(i)} \leftarrow \mathbf{r}^{i-1} + \beta_{i-1}\left(\mathbf{p}^{(i-1)} - \omega_{i-1}\mathbf{v}^{(i-1)}\right)$.

End If

End If

$\tilde{\mathbf{p}} \leftarrow \mathbf{M}^{-1}\mathbf{p}^{(i)}$.

$\mathbf{v}^{(i)} \leftarrow \mathbf{A}\tilde{\mathbf{p}}$.

$\alpha_i \leftarrow \frac{\rho_{i-1}}{\tilde{\mathbf{r}}^T\mathbf{v}^{(i)}}$.

$\mathbf{s} := \mathbf{r}^{(i-1)} - \alpha_i\mathbf{v}^{(i)}$.

$\tilde{\mathbf{s}} \leftarrow \mathbf{M}^{-1}\mathbf{s}$.

$\mathbf{t} \leftarrow \mathbf{A}\tilde{\mathbf{s}}$.

$\omega_i \leftarrow \frac{\mathbf{t}^T\mathbf{s}}{\mathbf{t}^T\mathbf{t}}$.

$\mathbf{x}^{(i)} \leftarrow \mathbf{x}^{(i-1)} + \alpha_i\tilde{\mathbf{p}} + \omega_i\tilde{\mathbf{s}}$.

$\mathbf{r}^{(i)} \leftarrow \mathbf{s} - \omega_i\mathbf{t}$.

End While

In Steps 18 and 22, $\mathbf{M}$ is the discrete form of complex shifted Laplacian-PML preconditioner $\mathcal{M}$, and it should be approximately inverted. Because computing $\mathbf{M}^{-1}$ is expensive, in order to avoid inverting $\mathbf{M}$ directly, it is chosen to solve two additional linear systems $\mathbf{M}\tilde{\mathbf{p}} = \mathbf{p}^{(i)}$ and $\mathbf{M}\tilde{\mathbf{s}} = \mathbf{s}$. In practice, these two linear systems do not have to be solved exactly, and an approximate solution will be enough. Of course, the preconditioning will be more efficient when the approximate solution is more exact. The multigrid method is employed to solve these additional linear systems in order to obtain a good approximate solution at a lower cost. Thus, the preconditioned Bi-CGSTAB algorithm takes Bi-CGSTAB method as an outer iteration and the multigrid method as an inner iteration. For convenience, we identify additional linear systems $\mathbf{M}\tilde{\mathbf{p}} = \mathbf{p}^{(i)}$ and $\mathbf{M}\tilde{\mathbf{s}} = \mathbf{s}$ with $\mathbf{Mu} = \mathbf{f}$. Now, we consider to solve the linear system $\mathbf{Mu} = \mathbf{f}$ with the multigrid method. For the multigrid, we have two basic cycles, one is the V-cycle and the other is W-cycle. We refer to a V-cycle with ν_1 relaxation sweeps before the correction step and ν_2 relaxation sweeps after the correction step as a V(ν_1, ν_2)-cycle, with a similar notation for W-cycle. The performance of V-cycle is generally poor while that of the W-cycle is too expensive. In practice, we use the full multigrid V-cycle (*FMG*), which possesses both the robustness of the W-cycle and the efficiency of the V-cycle. Similar to V(ν_1, ν_2), we have *FMG*(ν_1, ν_2).

As is known, multigrid methods degrade and diverge with increasing wavenumber k when solving the linear system stemming from the Helmholtz equation without any damping. However, an interesting observation is that the multigrid method converges satisfactorily for certain choices of β_1 and β_2 (see [18]). That is, it may be divergent for solving $\mathbf{Mu} = \mathbf{f}$ with the multigrid method when $(\beta_1, \beta_2) = (1, 0)$ in (2.10), while it is convergent when β_1, β_2 are properly chosen, especially β_2. Combining the suggestion in [10], we give the choice of β_2 in Section 4.1. In practice, *FMG*(2, 2) is chosen, the pointwise Jacobi relaxation with underrelaxation (ω-JAC) is used as a smoother, which is easy to parallel, and the coarse grid operators $M_{2h}, M_{4h}, \ldots$ are obtained by Galerkin principle. The advantage of the Galerkin coarse grid discretization is that the boundary conditions for coarse grid discretization do not need to be taken into consideration. For restriction operator, we choose full weighting operator instead of the transposition of the interpolation operator, which is commonly used but not absolutely necessary [10]. In fact, the full weighting operator performs much better for our problems. As for interpolation operator, the classic bilinear interpolation gives satisfactory convergence for constant coefficients and mildly varying wavenumbers, but for large wavenumbers and strongly varying coefficients, it is not robust enough. Here, we consider a matrix-based interpolation [8,22], which is constructed from the difference stencil, namely, according to the information stored in the coefficient matrix. As the interpolation operator can be computed in a black-box way, the corresponding multigrid is called the black-box multigrid. This kind of multigrid method is suitable for the uniform grid with difference scheme, and the problem we consider in this paper is in agreement with the situation.

In Fig. 5(a), the numbering in a difference stencil is presented. Fig. 5(b) shows one coarse and four fine grid cells with capital letters indicating coarse grid points and small letters indicating fine grid points. The fine grid denoted by Ω_h is split into four disjunct sub-grids $\Omega_{h,(0,0)}$, $\Omega_{h,(1,0)}$, $\Omega_{h,(0,1)}$, $\Omega_{h,(1,1)}$. $\Omega_{h,(0,0)}$ consists of the fine grid points which are also coarse grid points. $\Omega_{h,(1,0)}$ consists of the fine grid points which are located between two coarse grid points in the horizontal. $\Omega_{h,(0,1)}$ consists of the fine grid points which are located between two coarse grid points in the vertical, and the remaining grid points are denoted by $\Omega_{h,(1,1)}$. For example, $A, B, C, D \in \Omega_{h,(0,0)}$, $p, p^* \in \Omega_{h,(1,0)}$, $q, q^* \in \Omega_{h,(0,1)}$, and $r \in \Omega_{h,(1,1)}$. The symbols $\mathbf{e}_h, \mathbf{e}_H$ represent the grid functions for fine and coarse grids respectively. The corrections from coarse grids to fine grids are obtained by interpolation among the nearest coarse grid neighbors. For example, denote the interpolation weights at p by $W_C(p), W_D(p)$. Then, the correction for p is obtained by interpolation from C and D according to $W_C(p), W_D(p)$.

In [8], Zeeuw proposed a matrix-based interpolation operator which leaded to an efficient and robust black-box multigrid method for the convection–diffusion equation. Based on the Zeeuw's interpolation operator, many works obtained some efficient multigrid methods, such us in [31] for the diffusion equation and in [10] for the Helmholtz equation. In this text, we shall propose a new interpolation operator based on the symmetric and anti-symmetric parts of the coefficient matrix,

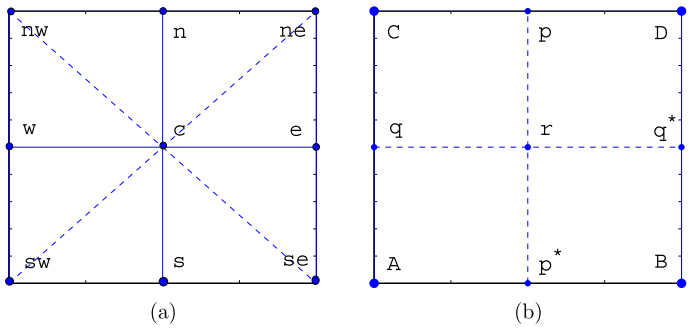

Fig. 5. (a) Nine point stencil with numbering. (b) Coarse and fine grid points, which are designated by capital and small letters respectively.

which is similar to the case of [8]. However, the symmetric part is assumed to originate from the Laplacian and zeroth terms and the anti-symmetric part is assumed to originate from the influence of PML, while the counterparts in [8] are considered to originate from the diffusion and convection terms. When constructing interpolation weights for p and q, lumped stencils are needed. For the symmetric part which is more important, the central element c in the stencil (Fig. 5(a)) is divided between the horizontal and vertical lumped stencils according to the contribution from the relative diffusion in horizontal and vertical directions respectively. For the anti-symmetric part, it is considered corresponding to the perturbation of the Laplacian due to PML. With the above strategies, it might lead to an efficient interpolation operator, especially for the case of varying wavenumbers, and this is illustrated by numerical examples in Section 4.

Now, we describe our novel interpolation operator. Since $\mathbf{M}$ is near-symmetric, we split it into a symmetric and an anti-symmetric parts. That is, let $\mathbf{M} = \mathbf{M}_s + \mathbf{M}_u$ with

$$\mathbf{M}_s := \frac{1}{2}(\mathbf{M} + \mathbf{M}^T), \qquad \mathbf{M}_u := \frac{1}{2}(\mathbf{M} - \mathbf{M}^T).$$

Let the stencil of $\mathbf{M}$ be

$$M^* := \begin{bmatrix} NW & N & NE \\ W & C & S \\ SW & S & SE \end{bmatrix}, \tag{3.1}$$

and let the corresponding stencils of $\mathbf{M}_s$ and $\mathbf{M}_u$ be

$$M_s^* := \begin{bmatrix} NW_s & N_s & NE_s \\ W_s & C_s & S_s \\ SW_s & S_s & SE_s \end{bmatrix} \quad \text{and} \quad M_u^* := \begin{bmatrix} NW_u & N_u & NE_u \\ W_u & C_u & S_u \\ SW_u & S_u & SE_u \end{bmatrix}, \tag{3.2}$$

respectively. Define $|M_s^*| := |NW_s| + |N_s| + |NE_s| + |W_s| + |C_s| + |E_s| + |SW_s| + |S_s| + |SE_s|$, and $|M_u^*|$ is similarly defined. Denote

$$\delta := \frac{|M_s^*|}{|M_s^*| + |M_u^*|}.$$

Now, we handle $\mathbf{M}_s$ and $\mathbf{M}_u$ respectively. First, we handle the stencil M_s^*. Denote $RS := NW_s + N_s + NE_s + W_s + C_s + E_s + SW_s + S_s + SE_s$ and $\tilde{C}_s := C_s - RS$. It can be seen that the stencil

$$\begin{bmatrix} NW_s & N_s & NE_s \\ W_s & \tilde{C}_s & E_s \\ SW_s & S_s & SE_s \end{bmatrix} \tag{3.3}$$

has no contribution from the Helmholtz zeroth-order term $(1 - \alpha i)k^2(x, y)$. Define θ_x and θ_y as

$$\theta_x := \frac{W_s + E_s}{N_s + S_s + W_s + E_s}, \qquad \theta_y := \frac{N_s + S_s}{N_s + S_s + W_s + E_s}. \tag{3.4}$$

Taking the Helmholtz zeroth-order term into account according to θ_x, θ_y, we obtain two lumped stencils both in the horizontal and vertical directions as follows

$$\begin{bmatrix} 0 & 0 & 0 \\ NW_s + W_s + SW_s & N_s + \tilde{C}_x + S_s & NE_s + E_s + SE_s \\ 0 & 0 & 0 \end{bmatrix}, \tag{3.5}$$

$$\begin{bmatrix} 0 & NW_s + N_s + NE_s & 0 \\ 0 & W_s + \tilde{C}_y + E_s & 0 \\ 0 & SW_s + S_s + SE_s & 0 \end{bmatrix}, \tag{3.6}$$

where $\tilde{C}_x = \tilde{C}_s + \theta_x \cdot RS$, and $\tilde{C}_y = \tilde{C}_s + \theta_y \cdot RS$. For the stencil M_u^*, we define

$$d_w := \max\big(|SW_u + W_u + NW_u|, |SW_u|, |W_u|, |NW_u|\big),$$
$$d_e := \max\big(|SE_u + E_u + NE_u|, |SE_u|, |E_u|, |NE_u|\big),$$
$$d_n := \max\big(|NW_u + N_u + NE_u|, |NW_u|, |N_u|, |NE_u|\big),$$
$$d_s := \max\big(|SW_u + S_u + SE_u|, |SW_u|, |S_u|, |SE_u|\big).$$

Then, the matrix-based interpolations, which determine the fine grid functions $\mathbf{e}_h$, are derived by the following algorithm.

Algorithm 3.2 *(The construction of interpolation).*

1. *For fine grid points* $A, B, C, D \in \Omega_{h,(0,0)}$ *(see Fig.* 5*), set*

$$\mathbf{e}_h(A) := \mathbf{e}_{2h}(A), \qquad \mathbf{e}_h(B) := \mathbf{e}_{2h}(B), \qquad \mathbf{e}_h(C) := e_{2h}(C), \qquad \mathbf{e}_h(D) := \mathbf{e}_{2h}(D).$$

2. *For fine grid points* $p \in \Omega_{h,(1,0)}$*, set*

$$W_C(p) := \delta\left|\frac{NW_s + W_s + SW_s}{N_s + \tilde{C}_x + S_s}\right| + (1-\delta)\frac{d_w}{d_w + d_e},$$
$$W_D(p) := \delta\left|\frac{NE_s + E_s + SE_s}{N_s + \tilde{C}_x + S}\right| + (1-\delta)\frac{d_e}{d_w + d_e},$$

and

$$\mathbf{e}_h(p) := W_C(p) \cdot \mathbf{e}_{2h}(C) + W_D(p) \cdot \mathbf{e}_{2h}(D).$$

3. *For fine grid points* $q \in \Omega_{h,(0,1)}$*, set*

$$W_A(q) := \delta\left|\frac{NW_s + N_s + NE_s}{W_s + \tilde{C}_y + E_s}\right| + (1-\delta)\frac{d_n}{d_n + d_s},$$
$$W_C(q) := \delta\left|\frac{SW_s + S_s + SE_s}{W_s + \tilde{C}_y + E_s}\right| + (1-\delta)\frac{d_s}{d_n + d_s},$$

and

$$\mathbf{e}_h(q) := W_A(q) \cdot \mathbf{e}_{2h}(A) + W_C(q) \cdot \mathbf{e}_{2h}(C).$$

4. *For fine grid points* $r \in \Omega_{h,(1,1)}$*, set*

$$W_A(r) := -\big(SW + W_A(p^*)S + W_A(q)W\big)/C,$$
$$W_B(r) := -\big(SE + W_B(p^*)S + W_B(q^*)E\big)/C,$$
$$W_C(r) := -\big(NW + W_C(p)N + W_C(q)W\big)/C,$$
$$W_D(r) := -\big(NE + W_D(p)N + W_D(q^*)E\big)/C,$$

and

$$\mathbf{e}_h(r) := W_A(r) \cdot \mathbf{e}_{2h}(A) + W_B(r) \cdot \mathbf{e}_{2h}(B) + W_C(r) \cdot \mathbf{e}_{2h}(C) + W_D(r) \cdot \mathbf{e}_{2h}(D).$$

We remark that the construction of the interpolation operator is based on the symmetric and anti-symmetric parts of $\mathbf{M}$. If $\mathbf{M}$ is symmetric, then $\delta = 1$, and RS can be considered to be the discretization of the Helmholtz zeroth-order term. For example, when M_s^* is the classical 5-point stencil, that is, $NW_s = NE_s = SW_s = SE_s = 0$, $N_s = W_s = E_s = S_s = -1$, $C_s = 4 - (1-\alpha i)k^2(x,y)$, then $RS = -(1-\alpha i)k^2(x,y)$ and $\tilde{C}_s = 4$. When constructing the horizontal lumped stencil (3.5) and the vertical lumped stencil (3.6), RS is redistributed to both of them according to the coefficients θ_x, θ_y. For the Laplacian, with classical 5-point stencil on fine gird without PML, the interpolation weights for p, q and r reduce to 1/2, 1/2, 1/4 respectively, which is just the bilinear interpolation. In this classical setting, the bilinear interpolation contributes to an efficient and robust multigrid, which is well known.

In Step 4 of Algorithm 3.2, $W_A(r), W_B(r), W_C(r), W_D(r)$ are determined such that the corresponding component of vector $\mathbf{M}\mathbf{e}_h$ at r is zero, which aims to prevent huge jumps of the norm of the residual after interpolation.

Table 4
Comparison for the different choice of β_2 at $k = 120$, $\alpha = 0$. ρ is the numerical multigrid convergence factor, N and t are the number of Bi-CGSTAB iterations and CPU time (s).

(β_1, β_2)	$(1, 0.3)$	$(1, 0.35)$	$(1, 0.4)$	$(1, 0.5)$	$(1, 0.7)$	$(1, 0.8)$	$(1, 1)$
ρ	3.25	2.06	1.28	0.66	0.34	0.32	0.28
N	–	33	25	28	33	36	43
t (s)	–	13.1	10.0	11.5	13.0	14.0	16.2

Table 5
The smoothing factors and the multigrid convergence factors from LAF for $(\beta_1, \beta_2) = (1, 0.5)$, $k = 120$, $\alpha = 0$ with ω-JAC ($\omega = 0.5$) smoother and the new interpolation operator.

(ν_1, ν_2)	$\mu(\Omega_1)$	$\mu(\Omega_2)$	$\mu(\Omega_3)$	μ	ρ_{2g}	ρ_{3g}
$(1, 1)$	0.8960	0.8851	0.8432	0.7432	0.7649	0.7876
$(2, 2)$	0.8132	0.7996	0.7225	0.5684	0.5830	0.5921

4. Numerical experiments

In this section, numerical experiments are given to demonstrate the performance of the preconditioned Bi-CGSTAB for solving the linear system (2.12) discretized from the Helmholtz-PML equation preconditioned with a complex shifted Laplacian-PML by an optimal 9-point difference scheme. The experiments also show the efficiency of the black-box multigrid with the newly proposed interpolation operator. Full multigrid V-cycle (*FMG*), which possesses both the robustness of the W-cycle and the efficiency of the V-cycle, is used, and *FMG*$(2, 2)$ is chosen. For the multigrid component, the ω-JAC ($\omega = 0.5$) method, the full weight restriction operator, the newly proposed interpolation operator and the Galerkin principle are used.

4.1. The Helmholtz-PML equation with constant wavenumber

A computational domain $\Omega = (0, 1) \times (0, 1)$ is considered, and a point source is located at the center of the domain. Applying the optimal 9-point difference scheme with stencil (2.22) to the Helmholtz-PML equation (2.3) yields the linear system (2.5). Then, we use the Bi-CGSTAB Algorithm 3.1 to solve the preconditioned linear system (2.12) with the complex shifted Laplacian-PML preconditioner (2.13). The preconditioned Bi-CGSTAB iteration terminates if the Euclidean norm of the relative residual error is reduced to the order of 10^{-6}. A zero initial guess has been used, and all the tests are performed on Intel(R) PC with 2.66 GHz and 4 Gb RAM.

We choose $\beta_1 = 1$ in operator $\mathcal{M}$. As to β_2, it should be chosen properly in order to achieve a faster speed for preconditioned Bi-CGSTAB. For smaller β_2, it is difficult to invert preconditioner $\mathbf{M}$ approximately with multigrid methods, and the preconditioned Bi-CGSTAB method will be inefficient. For larger β_2, it is easy to invert preconditioner $\mathbf{M}$ approximately, but the corresponding preconditioned system possesses an unfavorable spectral, which also weakens the efficiency. In Table 4, some different β_2 are evaluated for $k = 120$ and $\alpha = 0$. The notation N represents the number of preconditioned Bi-CGSTAB iterations, t denotes the CPU time in seconds, and ρ represents the numerical multigrid convergence factor for $\mathbf{Mu} = \mathbf{v}$, which is defined as

$$\rho := \lim_{n\to\infty} \sqrt[n]{\frac{\|\mathbf{v} - \mathbf{M}\mathbf{u}^n\|}{\|\mathbf{v} - \mathbf{M}\mathbf{u}^0\|}},$$

where n indicates the number of *FMG*$(2, 2)$ iteration, $\mathbf{u}^0$ is the initial guess, and $\mathbf{u}^n$ is the approximate solution at nth step. It is observed that when β_2 is small, such as $\beta_2 = 0.3$, both the multigrid and preconditioned Bi-CGSTAB diverge, and when $\beta_2 \geqslant 0.5$ both the multigrid and preconditioned Bi-CGSTAB converge, and more iterations will be needed with the increasing β_2. An interesting observation is that the preconditioned Bi-CGSTAB still converges while the multigrid diverges for $\beta_2 = 0.35$ and $\beta_2 = 0.4$. This is justified by the fact that though multigrid diverges, the effect of smoothing methods and the coarse-grid correction are just efficient in one *FMG*$(2, 2)$ iteration.

Fourier smoothing and two-grid analysis are two classical multigrid analysis tools [24,26], and a three-grid Fourier analysis was proposed in [33] to analyze the coarse-grid correction in some more detail. Since the success of multigrid is determined by a perfect interplay between smoothing and coarse-grid correction, we use a Local Fourier Analysis (LFA) tool to see the smoothing properties of the Jacobi smoother for PML and the coarse-grid correction process. General linear discrete operators with constant coefficients are considered in LFA. For discrete operators with nonconstant coefficients, such as the Helmholtz-PML equation, it can be replaced locally (by freezing the coefficients) by an operator with constant coefficients. For the LFA software, we refer to [34]. In Table 5, the smoothing factors and the multigrid convergence factors from LAF are presented for $(\beta_1, \beta_2) = (1, 0.5)$, $k = 120$, $\alpha = 0$ with ω-JAC ($\omega = 0.5$) smoother and the new interpolation operator. $\mu(\Omega_1)$, $\mu(\Omega_2)$ and $\mu(\Omega_3)$ represent the smoothing factors from the analysis for the discrete Helmholtz-PML operator in PML domains Ω_1, Ω_2 and Ω_3 respectively. μ, ρ_{2g} and ρ_{3g} represent the smoothing factor, two- and three-grid convergence

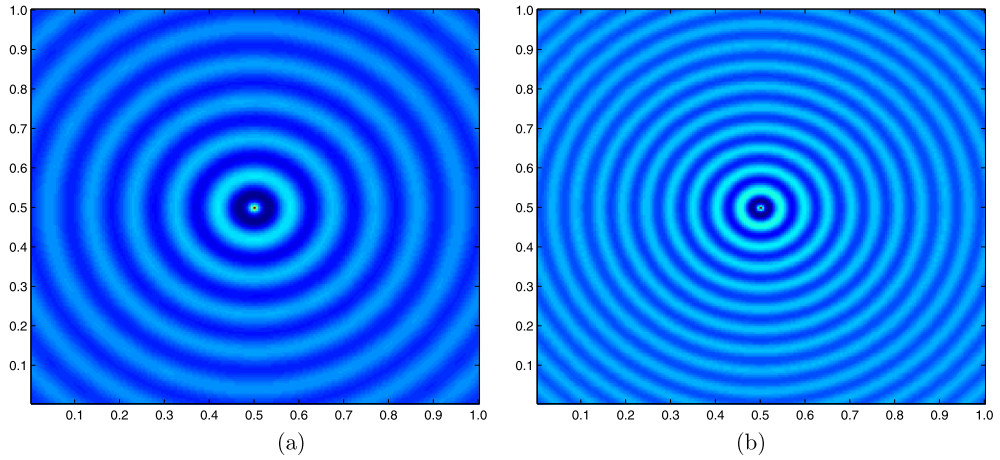

Fig. 6. (a) The real part of numerical solution at $k = 60$ without damping. (b) The real part of numerical solution at $k = 120$ without damping.

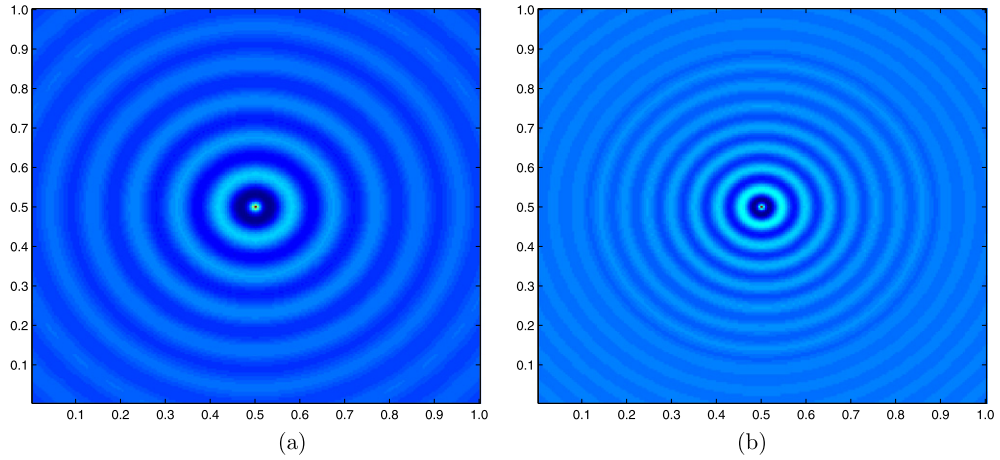

Fig. 7. (a) The real part of numerical solution at $k = 60$ with 5% damping ($\alpha = 0.05$). (b) The real part of numerical solution at $k = 120$ with 5% damping ($\alpha = 0.05$).

factors from the analysis for the discrete Helmholtz-PML operator in interested domain Ω_0. As can be seen, the smoothing factors corresponding to the PML domain are larger than that corresponding to the interested domain. It is also observed that there is a small difference between the two- and three-grid convergence factors, which indicates a favorable coarse correction.

We choose $(\beta_1, \beta_2) = (1, 0.5)$ as a basic parameter for computation, which is a proper choice. The numerical solutions corresponding to $k = 60$ and $k = 120$ are presented in Figs. 6 and 7, where there is no physical reflection at the boundaries due to the PML.

Let G be the number of gridpoints per wavelength, and an accuracy requirement for second-order discretizations is that $kh \leqslant 2\pi/G$. We set $G = 8$, $kh \approx 2\pi/G = \pi/4$, and Tables 6 and 7 show the number of preconditioned Bi-CGSTAB iterations and CPU time (in parentheses) in seconds with and without damping for different wavenumbers, respectively. Table 6 is for the low and moderate wavenumbers, and Table 7 is for the high wavenumbers. The largest wavenumber for test is $k = 900$, and the number of unknowns (without PML) is $1147 \times 1147 = 1\,315\,609$. (I), (II), (III) represent the preconditioned BI-CGSTAB methods based on multigrid with bilinear interpolation operator, the interpolation operator suggested in [10], and the new interpolation operator proposed in this paper respectively. As can be seen, the method (III) gains a faster convergence than methods (I) and (II). For $k = 900$, without damping, it needs 313 iterations for (III), and the time-consuming is 1013 s. It can also be seen that the convergence speed with some damping in the Helmholtz problem is considerably faster than that without damping, which can be expected from the spectral distribution in Fig. 4(f). This indicates that the damping will improve the property of Helmholtz equation. Some damping is significant in the actual geophysics application.

Tables 6 and 7 present the convergence of the preconditioned BI-CGSTAB method for $G = 8$. We also present the convergence of the preconditioned BI-CGSTAB method with the new interpolation operator for $G = 6, 7, 9, 10$ in Table 8, where some different wavenumbers are evaluated without damping. $G = 6, 7$ correspond to the grid coarsening, and $G = 9, 10$ correspond to grid refinement. It is observed that when less gridpoints per wavelength are used, the less CPU time (in

Table 6
Number of Bi-CGSTAB iterations and CPU time in seconds (in parentheses) for low and moderate wavenumbers k with and without damping.

		$k = 50$	$k = 80$	$k = 120$	$k = 150$	$k = 240$
		Grid				
		65×65	103×103	154×154	192×192	307×307
(I)	$\alpha = 0.00$	22 (0.34)	32 (1.00)	46 (2.99)	61 (5.89)	91 (22.7)
	$\alpha = 0.01$	20 (0.31)	26 (0.88)	35 (2.27)	46 (4.43)	67 (16.7)
(II)	$\alpha = 0.00$	19 (0.29)	26 (0.87)	40 (2.60)	54 (5.20)	81 (20.2)
	$\alpha = 0.01$	18 (0.28)	24 (0.81)	32 (2.08)	40 (3.85)	56 (14.0)
(III)	$\alpha = 0.00$	16 (0.25)	23 (0.78)	33 (2.14)	45 (4.34)	69 (17.1)
	$\alpha = 0.01$	15 (0.23)	22 (0.74)	28 (1.82)	33 (3.18)	48 (11.9)

Table 7
Number of Bi-CGSTAB iterations and CPU time in seconds (in parentheses) for high wavenumbers k with and without damping.

		$k = 600$	$k = 700$	$k = 800$	$k = 900$
		Grid			
		765×765	893×893	1020×1020	1147×1147
(I)	$\alpha = 0.00$	231 (338.1)	312 (616.8)	378 (972.4)	424 (1373)
	$\alpha = 0.01$	99 (145.3)	122 (241.8)	124 (319.5)	143 (463.2)
(II)	$\alpha = 0.00$	200 (292.6)	255 (504.3)	293 (754.7)	356 (1152)
	$\alpha = 0.01$	89 (130.5)	101 (200.0)	110 (283.4)	133 (431.0)
(III)	$\alpha = 0.00$	175 (255.8)	225 (446.7)	254 (655.6)	313 (1013)
	$\alpha = 0.01$	78 (116.5)	88 (176.0)	93 (240.1)	116 (376.4)

Table 8
Number of Bi-CGSTAB iterations and CPU time in seconds (in parentheses) for $G = 6, 7, 9, 10$ at different wavenumbers k without damping.

	$k = 50$	$k = 80$	$k = 120$	$k = 150$	$k = 250$	$k = 600$
$G = 6$	15 (0.16)	21 (0.58)	32 (1.47)	43 (2.83)	65 (9.70)	168 (148.5)
$G = 7$	15 (0.20)	22 (0.70)	32 (1.96)	44 (3.83)	67 (13.9)	172 (208.4)
$G = 9$	15 (0.28)	23 (1.08)	34 (3.06)	46 (6.13)	71 (23.4)	178 (345.8)
$G = 10$	16 (0.31)	25 (1.38)	35 (3.78)	48 (8.01)	74 (29.8)	183 (438.3)

seconds) is needed for the same wavenumbers, and vice versa. This is the reason why we adopt the optical 9-point difference scheme which needs less gridpoints per wavelength than the conventional 5-point scheme while maintaining the comparable accuracy.

4.2. The cave model

The cave model is used to evaluate the preconditioned Bi-CGSTAB for a simple heterogeneous medium. We consider the domain which is defined to be a rectangle of dimension 3000×4000 m^2. A point source is located at point (1200 m, 2000 m), and the upper surface is assigned to be $y = 0$. Fig. 8 presents the domain, the cave, and the variation of speed in the medium. The blue, green, and red parts represent 1600 m/s, 2000 m/s, 2400 m/s respectively in Fig. 8(a). The real part of the numerical solution at $f = 30$ Hz without damping is plotted in Fig. 8(b). Table 9 presents the convergence results of preconditioned Bi-CGSTAB for different frequencies (varying from 10 Hz to 60 Hz) with and without damping. The number of Bi-CGSTAB iterations and CPU time in seconds (in parentheses) are presented. As in Section 4.1, (I), (II), (III) represent the preconditioned BI-CGSTAB based on multigrid with bilinear interpolation operator, the interpolation operator suggested in [10], and the new interpolation operator proposed in this paper respectively. As can be seen, all of the three interpolation operators perform robustly, while method (III) still achieves a faster convergence than methods (I) and (II). Still, the convergence speed of the Helmholtz problem with some damping is considerably faster than that without damping.

4.3. The salt dome model

The salt dome model mimics the subsurface geology under the sea, which shows a more complicated heterogeneous medium. We consider the domain which is defined to be a rectangle of dimension $4800 \times 16\,000$ m^2. A point source is located at point (2250 m, 8000 m) under the surface. Fig. 9(a) presents the domain, the salt dome, and the variation of speed in the medium. The values for the speed of sound are irregularly structured throughout the domain. The real part of the numerical solution at $f = 40$ Hz without damping is plotted in the right figure. Table 10 presents the preconditioned Bi-CGSTAB convergence results for the case with and without damping for different frequencies, which varies from 10 Hz to

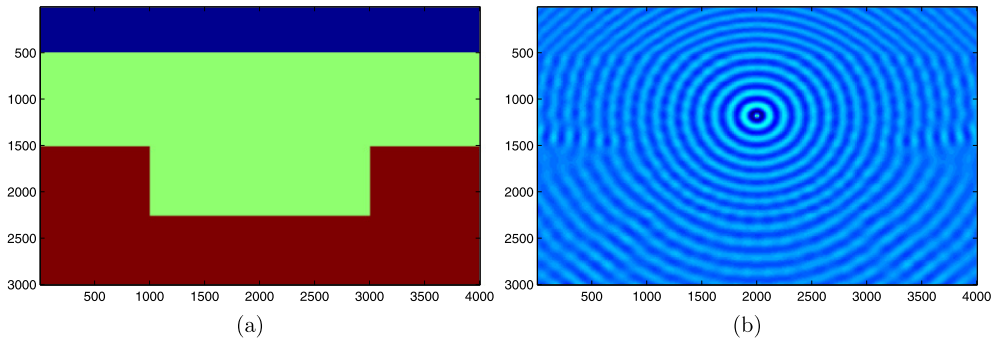

Fig. 8. (a) The cave problem with speed profile indicated. (b) The real part of numerical solution at $f = 30$ Hz. (For interpretation of colors in this figure, the reader is referred to the web version of this article.)

Table 9
Bi-CGSTAB convergence for the cave model with and without damping. The number of Bi-CGSTAB iterations and CPU time in seconds (in parentheses).

f (Hz)	Grid	α	(I)	(II)	(III)
10	161×121	0.00	46 (2.85)	45 (2.78)	34 (2.05)
		0.01	39 (2.40)	35 (2.16)	30 (1.88)
20	334×251	0.00	192 (45.9)	86 (20.6)	68 (16.6)
		0.01	132 (31.4)	61 (14.8)	49 (11.9)
30	435×327	0.00	134 (51.8)	111 (42.9)	95 (36.7)
		0.01	84 (32.5)	70 (27.1)	60 (23.9)
40	572×429	0.00	198 (130.2)	150 (98.3)	130 (85.2)
		0.01	87 (57.0)	77 (50.5)	67 (44.0)
50	690×518	0.00	191 (180.0)	172 (162.1)	148 (139.4)
		0.01	88 (82.1)	85 (80.8)	73 (68.9)
60	870×653	0.00	292 (440.2)	212 (320.7)	184 (278.4)
		0.01	113 (170.0)	95 (143.2)	82 (124.5)

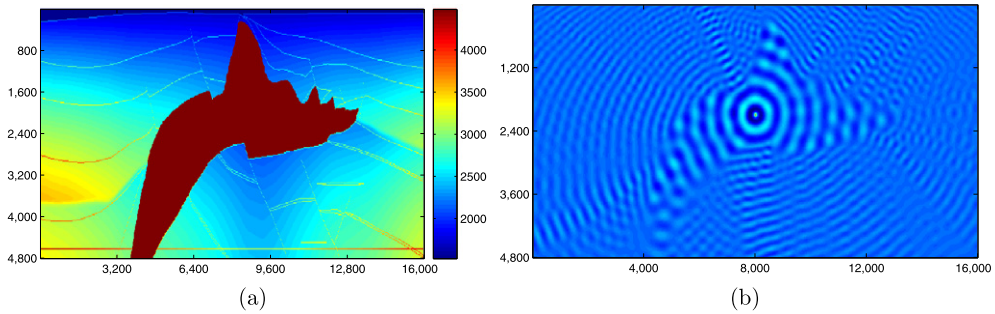

Fig. 9. (a) The salt dome problem with velocity profile indicated. (b) The real part of numerical solution at $f = 40$ Hz.

35 Hz. The number of Bi-CGSTAB iterations and CPU time in seconds (in parentheses) are shown. In Table 10, '> 500' means that it needs more than 500 iterations for the preconditioned Bi-CGSTAB method to reduce the relative residual to 10^{-6}. We can see that the bilinear interpolation operator (I) is not robust enough with the increasing frequency, while methods (II), (III) are robust. (III) gains a faster convergence speed than methods (I) and (II).

5. Conclusions

In this paper, we use the complex shifted Laplacian-PML preconditioner to the Helmholtz-PML equation. We first analyze the spectral distribution of the system discretized from the preconditioned Helmholtz-PML equation by an optimal 9-point difference scheme. We illustrate the approximately moon-shaped spectrum which is enclosed by certain circle from the perspective of linear fractional map in complex variable function. We also make a series of numerical experiments which help to prove numerically that there holds the sufficient and necessary condition for the spectrum being enclosed by certain circle. Then, we propose a new interpolation operator for multigrid-based preconditioned Krylov subspace method. We refer to the matrix-based multigrid with the new interpolation operator as a new multigird. The numerical experiments show the efficiency of the preconditioned Bi-CGSTAB with the new multigrid. It also presents a faster convergence of the

Table 10
Bi-CGSTAB convergence for the salt dome problem with and without damping. Iterations and CPU time in seconds (in parentheses) are shown.

f (Hz)	Grid	α	(I)	(II)	(III)
10	180×600	0.00	267 (81.7)	59 (18.5)	50 (15.8)
		0.01	180 (55.1)	47 (14.2)	41 (12.2)
15	240×800	0.00	113 (59.8)	81 (42.2)	69 (36.6)
		0.01	68 (36.0)	54 (28.9)	45 (28.4)
20	300×1000	0.00	> 500	122 (99.9)	103 (84.6)
		0.01	420 (343)	69 (56.5)	58 (47.0)
25	360×1200	0.00	> 500	140 (167.5)	120 (143.7)
		0.01	> 500	77 (92.7)	65 (77.8)
30	423×1412	0.00	> 500	185 (303.9)	162 (266.1)
		0.01	> 500	94 (154.4)	81 (133.6)
35	514×1714	0.00	> 500	261 (650.8)	227 (566.4)
		0.01	> 500	103 (256.8)	88 (219.9)

preconditioned Bi-CGSTAB with the new interpolation operator. The application ranges from constant wavenumbers to irregular heterogeneity structures in a medium. The new multigrid-based preconditioned Bi-CGSTAB method for Helmholtz-PML equation is proved to be an efficient and robust iterative method.

References

[1] I. Babuška, F. Ihlenburg, E.T. Paik, S.A. Sauter, A generalized finite element method for solving the Helmholtz equation in two dimensions with minimal pollution, Comput. Methods Appl. Mech. Engrg. 128 (1995) 325–359.
[2] A. Bayliss, C.I. Goldstein, E. Turkel, An iterative method for Helmholtz equation, J. Comput. Phys. 49 (1983) 631–644.
[3] J.P. Bérenger, A perfectly matched layer for the absorption of electromagnetic waves, J. Comput. Phys. 114 (1994) 185–200.
[4] M. Benzi, Preconditioning techniques for large linear systems: A survey, J. Comput. Phys. 182 (2002) 418–477.
[5] W.L. Briggs, V.E. Henson, S.F. McCormick, A Multigrid Tutorial, second ed., SIAM, California, 2000.
[6] Z. Chen, D. Cheng, W. Feng, T. Wu, An optimal 9-point finite difference scheme for the Helmholtz equation with PML, preprint.
[7] W.C. Chew, J.M. Jin, E. Michielssen, Complex coordinate stretching as a generalized absorbing boundary condition, Microwave Opt. Technol. Lett. 15 (1997) 363–369.
[8] P.M. De Zeeuw, Matrix-dependent prolongations and restrictions in a blackbox multigrid solver, J. Comput. Appl. Math. 33 (1990) 1–27.
[9] Y.A. Erlangga, C. Vuik, C.W. Oosterlee, On a class of preconditioners for the Helmholtz equation, Appl. Numer. Math. 50 (2004) 629–651.
[10] Y.A. Erlangga, C.W. Oosterlee, C. Vuik, A novel multigrid based preconditioner for heterogeneous Helmholtz problems, SIAM J. Sci. Comput. 27 (2006) 1471–1492.
[11] Y.A. Erlangga, C. Vuik, C.W. Oosterlee, Comparison of multigrid and incomplete LU shifted-Laplace preconditioners for the inhomogeneous Helmholtz equation, Appl. Numer. Math. 56 (2006) 648–666.
[12] J. Gozani, A. Nachshon, E. Turkel, Conjugate gradient compiled with multigrid for an indefinite problems, in: R. Vichnevestsky, R.S. Tepelman (Eds.), Advances in Computer Methods for Partial Differential Equation, vol. V, IMACS, New Brunswick, NJ, 1984, pp. 425–427.
[13] P.R. Graves-Morris, The breakdowns of Bi-CGSTab, Numer. Algorithms 29 (2002) 97–105.
[14] F.D. Hastings, J.B. Schneider, S.L. Broschat, Application of the perfectly matched layer (PML) absorbing boundary condition to elastic wave propagation, J. Acoust. Soc. Amer. 100 (1996) 3061–3069.
[15] A.S. Householder, The Theory of Matrices in Numerical Analysis, Blaisdell Publishing Company, New York, 1964.
[16] F. Ihlenburg, I. Babuška, Dispersion analysis and error estimation of Galerkin finite element methods for the Helmholtz equation, Internat. J. Numer. Methods Engrg. 38 (1995) 4207–4235.
[17] C. Jo, C. Shin, J. Suh, An optimal 9-point, finite-difference, frequency-space, 2-D scalar wave extrapolator, Geophysics 61 (1996) 529–537.
[18] S. Kim, Multigrid simulation for high-frequency solutions of the Helmholtz problem in heterogeneous Helmholtz media, SIAM J. Sci. Comput. 24 (2002) 684–701.
[19] A.L. Laird, M.B. Giles, Preconditioned iterative solution of the 2D Helmholtz equation, Report 02/12, Oxford Computer Laboratory, Oxford, UK, 2002.
[20] C.D. Riyanti, A. Kononov, Y.A. Erlangga, C. Vuik, C. Oosterlee, R.E. Plessix, W.A. Mulder, A parallel multigrid-based preconditioner for the 3D heterogeneous high-frequency Helmholtz equation, J. Comput. Phys. 224 (2007) 431–448.
[21] Y. Saad, W.H. Schultz, GMRES: A generalized minimal residual algorithm for solving nonsymmetric linear system, SIAM J. Sci. Statist. Comput. 7 (1986) 1–176.
[22] Y. Shapira, Analysis of matrix-dependent multigrid algorithms, Numer. Linear Algebra Appl. 5 (1998) 165–201.
[23] I. Singer, E. Turkel, A perfectly matched layer for the Helmholtz equation in a semi-infinite strip, J. Comput. Phys. 201 (2004) 439–465.
[24] K. Stüben, U. Trottenberg, Multigrid methods: Fundamental algorithms, model problem analysis and applications, in: W. Hackbusch, U. Trottenberg (Eds.), Multigrid Methods, in: Lecture Notes in Math., vol. 960, Springer-Verlag, Berlin, 1982, pp. 1–176.
[25] I. Stekl, R.G. Pratt, Accurate viscoelastic modeling by frequency-domain finite differences using rotated operators, Geophysics 63 (1998) 1779–1794.
[26] U. Trottenberg, C.W. Oosterlee, A. Schäller, Multigrid, Academic Press, New York, 2001.
[27] S. Tsynkov, E. Turkel, A cartesian perfectly matched layer for the Helmholtz equation, in: L. Tourrette (Ed.), Artificial Boundary Conditions, with Applications to CFD Problems, Nova Science Publishers Inc., Commack, NY, 2000.
[28] N. Umetani, S.P. MacLachlan, C.W. Oosterlee, A multigrid-based shifted Laplacian preconditioner for a fourth-order Helmholtz discretization, Numer. Linear Algebra Appl. 16 (2009) 603–626.
[29] H.A. Van Der Vorst, Bi-CGSTAB: A fast and smoothly converging variant of Bi-CG for the solution of nonsymmetric linear systems, SIAM J. Sci. Statist. Comput. 13 (1992) 631–644.
[30] M.B. Van Gijzen, Y.A. Erlangga, C. Vuik, Spectral analysis of the discrete Helmholtz operator with a shifted Laplacian, SIAM J. Sci. Comput. 29 (2007) 1942–1958.
[31] T. Washio, W. Oosterlee, Flexible multiple semicoarsening for three-dimensional singularity perturbed problems, SIAM J. Sci. Comput. 19 (1998) 1646–1666.

[32] P. Wesseling, An Introduction to Multigrid Methods, Library of Congress Cataloging-in-Publication Data, USA, 2004.
[33] R. Wienands, C.W. Oosterlee, On three-grid Fourier analysis for multigrid, SIAM J. Sci. Comput. 23 (2001) 651–671.
[34] R. Wienands, Local Fourier Analysis (LFA) for two-dimensional scalar partial differential equations, available from: http://www.mgnet.org/mgnet-codes-wienands.html.
[35] S. Wu, T. Huang, L. Li, L. Xiong, Positive stable preconditioners for symmetric indefinite linear systems arising form Helmholtz equations, Phys. Lett. A 373 (2009) 2401–2407.